Vibration Isolation of Sensitive Equipment Using Cohesionless Soil

BY

JAYSON WJ ANTON
B.S., Oregon State University, 2005

THESIS

Submitted as partial fulfillment of the requirements
for the degree of Doctor of Philosophy in Mechanical Engineering
in the Graduate College of the
University of Illinois at Chicago, 2018

Chicago, Illinois

Defense Committee:

Thomas Royston, Chair and Advisor
Ahmed Shabana
Michael Scott
Deming Shu, Argonne National Laboratory
Curt Preissner, Argonne National Laboratory

This thesis is dedicated to my daughter, Beatrice Joan Anton-Westing.

ACKNOWLEDGMENTS

I would like to, first and foremost, thank my partner Corrie Westing CNM. She has been there for me every step of the way. She has supported and encouraged me all along the way, and continues to inspire me in all her pursuits.

Thank you to my advisor, Professor Thomas J. Royston. He has been there to patiently answer all my questions and guide me through any technical problems I had during my research. A special thank you is in order for Dr. Deming Shu at the Advanced Photon Source for being my co-advisor. He has shared so much of his incredible wealth of knowledge with me. I would not have come to the APS nor would I have stayed had it not been for Deming. I am thankful to Dr. Curt Preissner for being a mentor and giving me valuable advice about the technical aspects of my research as well as advice about the personal side of a dissertation. Thank you to Professor Ahmed A. Shabana and Professor Michael Scott for their insights into my research as members of my defense committee.

In addition, I would like to thank some more people at Argonne National Laboratory who have help along the way. Dr. Steven Kearney for helping in the data collection process and for his advice on writing a thesis at UIC. Nathan Guisinger, Ron Tollner, Brandon Fisher, and Scott Massow for helping with access to and architectural data on the Center for Nanoscale Materials.

I would like to thank Harish Palnitkar, Altaf Kahn, Zoujun Dai, Ying Peng, Yifei Liu, and Brian Henry, at the Acoustics and Vibration Laboratory at UIC for assisting me in getting access to and technical support of Comsol Multiphysics finite element software. A special thank you to Wanda Flores in the MIE office for helping me navigate the process of submitting and defending my dissertation.

I am very grateful to Laurel Spindel LCSW for helping me find my strengths and overcome my weaknesses allowing me to complete this process.

JWJA

TABLE OF CONTENTS

LIST OF TABLES

TABLE **PAGE**

LIST OF FIGURES

FIGURE **PAGE**

SUMMARY

This dissertation is an investigation of cohesionless soils in vibration isolation structures. The goal of this dissertation is to propose designs for vibration isolation structures that meet strict stability requirements of the high-precision machines to be used on them.

This was done through careful experimental measurements on a variety of structures with various cohesionless soils under a range of conditions. Analytical models were used to find dynamic parameters for the soils from the experimental data. These parameters were compared to existing theories of cohesionless soil mechanics and were seen to be in relatively good agreement.

Using the appropriate theories finite element (FE) models were created that could predict the dynamic behavior of the structures. Careful consideration of factors such as boundary conditions, mesh element size, and shunting were undertaken to improve the accuracy of the FE models

From these models an understanding of what key parameters affect the ability of these structures to isolate sensitive equipment from vibrational disturbances could be ascertained. Proposals for the design of vibration isolation structures that are appropriate for their use and location are then proposed.

1 INTRODUCTION

1.1 The Purpose

There are two vibration isolation strategies currently being used at Argonne National Laboratory incorporating cohesionless soil. The first is incorporating sand into a combined vibration-damping (CVD) structure as part of the footings for instrumentation tables. The second is a series of rectangular pits, embedded in grade, filled with sand or gravel, and capped with concrete for the mounting of electron microscopes.

The focus of this dissertation is to understand the dynamic behavior of cohesionless soil in these structures to build robust predictive models. These models may help in gaining an understanding of what key parameters affect the ability of these structures to isolate sensitive equipment from vibrational disturbances. Designs for future pits and CVD structures will be proposed for use at Argonne National Laboratory to meet the strictest of stability requirements.

1.2 The Problem

With advancements in nanotechnology, silicon chip manufacturing, and x-ray imaging stricter and stricter vibration stability requirements are needed. The problem investigated in this dissertation is to use an understanding the dynamic behavior of cohesionless soils in vibration isolation structures in order to design structures to meet the strictest of stability requirements. To do this the following work was undertaken:

1.2.1 Sand as part of combined vibration-damping (CVD) footing structure

- Objective 1: Generate force response functions from experimental footing model
- Objective 2: Determine dynamic characteristics of sand using analytical models and experimental data

- Objective 3: Design a finite element model that predicts the dynamic behavior of the footing structures
- Objective 4: determine best configuration of sand in a CVD to isolate environmental noise at the APS

1.2.2 Filled Pits

- Objective 1: Understand current performance of filled pits by a comparison of ambient vibration levels on the pits to the surrounding floor and standard vibration criteria
- Objective 2: Design a finite element model of pits using impact data test data
- Objective 3: Use parametric studies of the pits to determine the best design for isolating environmental noise at the CNM

1.3 Novel Contributions to the Advancement of the Art

Various floor structures have been designed and studied to minimize vibration disturbances. The mechanics of cohesionless soil has also been extensively studied. But, the role cohesionless soil plays in these structures has not been studied in the literature. Through combining soil mechanics, vibration analysis of experimental data, analytical modeling, and finite element (FE) modeling this dissertation study expands the current body of knowledge on the vibration isolation of sensitive equipment.

1.4 Background and Motivation

This project focuses on two vibration isolation strategies currently in use at Argonne National Laboratory. The first is incorporating sand into a combined vibration-damping (CVD) structure as part of the footings for instrumentation tables. The CVD structures are in use at The Advanced Photon Source (APS). The second is a series of rectangular pits, embedded in grade, filled with sand or gravel, and capped with concrete for the mounting of electron microscopes. The embedded pits are located in a

Figure 1: "Advanced Photon Source AERIAL"
by John Hill licensed under
https://creativecommons.org/licenses/by-nc-sa/2.0/

building constructed specifically for electron microscopy of nanoscale materials at the Center for Nanoscale Materials (CNM). Some background about the operations at the APS and the CNM will help understand the motivation for this work.

1.4.1 The Advanced Photon Source

The APS, shown in Figure 1, is a synchrotron radiation source that offers a broad array of X-ray imaging opportunities such as, X-ray scattering, diffraction, and spectroscopy. Both soft X-rays (3-5 keV) and hard X-rays (up to 100 keV or higher) are produced at the beamlines. The APS currently has beamlines that offer spatial resolutions in the 10s of nanometers range (Advanced Photon Source n.d.).

The APS Upgrade, currently underway, will produce brighter and higher energy X-ray beams. These upgraded beams with advancements in X-ray optics new opportunities in X-ray microscopy will be available. One such opportunity is hard X-ray scanning probe with potential imaging down to 5 nm. Another is the ability to produce nanofocused beams with intensity two to three orders of magnitude

higher than at present sources (Streiffer 2015). These upgraded techniques with require even stricter stability requirements to reach their potential.

The CVD structures with sand are located at the 2-ID-D beamline and have been shown to meet the spatial resolution requirements of the x-ray microprobe located there (Xu 2002). At that beamline the feet of the optical table supporting the x-ray microprobe were placed atop a layer of sand enclosed on its sides by a steel box.

1.4.2 Center for Nanoscale Materials

The CNM is a user facility focused on nanoscience and nanotechnology. The facility provides instrumentation, expertise, and infrastructure to perform basic research for energy-related research and development programs. The CNM's Quantum and Energy Materials group uses ultrahigh-vacuum scanning-probe microscopies with a variety of capabilities to further this research in energy technologies at the atomic scale (Argonne National Laboratory n.d.).

Electron microscopy at the CNM is housed in building constructed specially for this purpose. The building is 34.2 m long by 11.6 meters wide and a ceiling high enough to accommodate structures up to 6.7 m tall. The floor of the facility is a continuous slab of 30.5 cm thick reinforced concrete. The

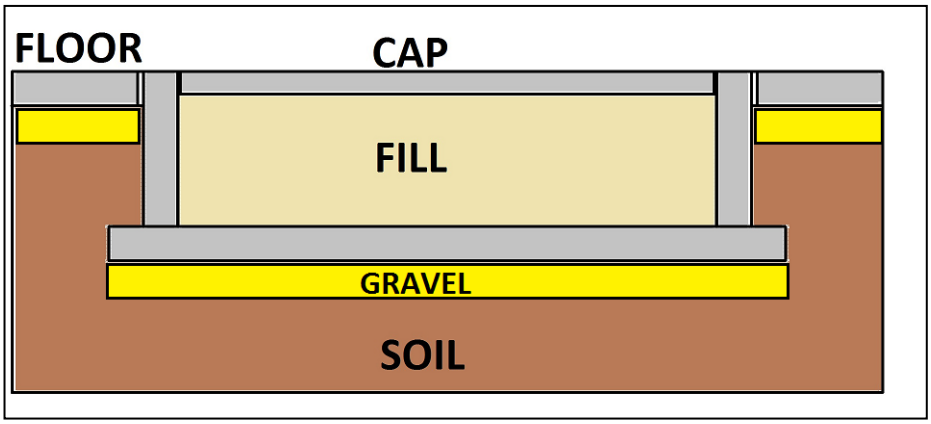

Figure 2: Cross section of filled pits at the Center for Nanoscale Materials

floor is isolated from the pits, concrete grade beams and the neighboring Advanced Photon Source building by 5.1 cm horizontal joint seal that is, or is equivalent to, EMSEAL Colorseal®. The concrete was poured on top of 30.5 cm of compacted CA6 gravel (R. Tollner, personal communication, April 17, 2013). The building is situated entirely in Ozaukee silt loam soil (Soil Survey Staff 2016).

During the facilities construction four 3.9 m wide by 4.8 m long by 1.4 m deep concrete pits were installed (see Figure 2). The pits consist of a 4.5 m wide by 5.4 long by 30.4 cm thick reinforced concrete slab on 30.4 cm of compacted CA6 gravel and 30.4 cm thick walls.

Two of the pits (Pit 1 and Pit 4) have been filled with commercially available play sand and then capped with a 15.24 cm reinforced concrete slab. Another, Pit 2, was filled with rounded pea gravel. It was then capped with a 38.1 cm reinforced concrete slab. The electron microscopes were then installed on the filled and capped pits. The final pit (Pit 3) has yet to be filled. This design approach was taken to incorporate vibration isolation effects similar to the isolated slab-on-grade and inertial slab techniques. It is also believed that materials like sand and gravel will add an extra damping effect on environmental noise.

2 Review of Pertinent Literature

2.1 Isolation of Vibration-Sensitive equipment

Nanotechnology research, metrology, microscopy, X-ray imaging, and silicon chip manufacturing all use precision equipment that is sensitive to vibrations. Therefore, many strategies have been studies for the isolation vibration-sensitive equipment from vibrational energy present in the surrounding environment. Such strategies include thick isolated concrete slab-on-grade (O'Keefe 2004), rigid "waffle" floor structures (Amick 1992), and pneumatically isolated inertia slabs (Amick 2002). Also, many materials are used in vibration isolation: metal springs, rubber isolators, air spring-dampers, and magnetic springs (Macinante 1984).

Other factors such as temperature, humidity, and air flow also need to be controlled (Soueid 2005 and O'Keefe 2004). These factors, however, are beyond the scope of this study.

Vibrational noise is what was studied in this dissertation. Many sources of vibration can affect sensitive equipment. The effect of construction (Amick 2000), automobile traffic (Hao 2001 and Lak 2011), and train traffic (Ju 2004, Ju 2007, and Costa 2012) on facilities and the sensitive equipment has on them have all been studied. Construction near facilities with vibration-sensitive equipment is sometimes unavoidable; study of the propagation of vibrational energy by construction equipment has been important. Automobile traffic induces vibrational energy at high frequencies. However, low frequency vibrations still have a greater effect on the vibration levels seen in buildings. Ju and Costa suggest ways of modeling train traffic induced vibrations and their effect on nearby buildings. Ju also makes recommendation for isolating buildings from such vibration such as retaining walls, pile foundations, and soil improvements.

Amick, Gordon, and Soueid have developed criteria for evaluating how suitable facilities are for the operation of vibration-sensitive equipment. Soueid and Amick developed the NIST-A criterion to meet the demands of the NIST Advance Measurement Laboratory (Soueid 2005). The NIST-A criterion

consists of two portions. The first requires vibration levels between 1 and 20 Hz to be below a constant rms displacement of 25 nm in 1/3 octave bands. From 20 Hz to 100 Hz rms vibration levels in 1/3 octave bands need to be below 3.1 μm/s from 20 Hz to 100 Hz.

The Generic Vibration Criteria, or VC, curves were developed by Gordin and Amick for use in the microelectronic, medical, and biopharmaceutical industries. The VC curves again use the standard 1/3 octave bands and originally had a frequency range of 4 to 80 Hz but has since been expanded to 1 to 80 Hz for newer curves (Gordon 1992). The criteria are a set of curves from VC-A, the most compliant, to VC-G, the strictest. To meet VC-A and VC-B vibration levels must be below a constant rms acceleration from 4 to 8 Hz (260 μg and 130 μg, respectively) and then a constant rms velocity from 8 to 80 Hz (50 and 25 micro-m/s, respectively) The VC-C through VC-G curves all require rms velocity levels to be below a constant velocity (Amick 2005).

2.2 Foundation-Soil Interaction

Understanding the dynamics of rigid foundations and what parameters of the soil it is placed on affect the dynamics is an import part of this study. Parameters of soil and their effects on foundation dynamics that have been studied in the literature including the shape of the foundation, surface and embedded foundations, and homogeneous half space and layered soils.

George Gazetas's paper "Analysis of machine foundation vibrations: state of the art" is foundational to this area of study (Gazetas 1983). In this a review of theory up to that point is made and then formulae for the vertical, horizontal, torsional, and rocking stiffness of soil for round and strip foundations, surface and embedded foundation, foundations on a stratum over a rigid and non-rigid halfspace. Dobry and Gazetas refine this this theory to include arbitrarily shaped foundation, dynamic stiffnesses, and damping values (Dobry 1986). Gazetas further expands the theory of dynamic stiffnesses and damping to embedded arbitrarily shaped foundations (Gazetas 1991a).

These theories were compared to data from 54 free vibration tests of embedded model footings and were generally confirmed (Gazetas 1991b). Baidya and Muralikrishna conducted a systematic analysis of experimental data of foundations on a layered medium (Baidya 2006). Their results found encouraging agreement between theory and experiments.

Other soil/foundation configurations have been investigated in the literature. A two-layered soil system over a rigid layer was experimentally investigated and it was found that a mass-spring-dashpot model can compare well to experimental results (Mandal 2012). A theoretical study was conducted of block foundations on layered soils (Kumar 2013). From this study it is concluded that with an increase in the ratio of soil layer depth over foundation width natural frequency and displacement amplitudes decrease.

Ashoori and Kim studied foundations on the surface of embedded in sand specifically. Kim experimentally studied rigid foundations on the surface of sand and proposed a distributed spring model with the stiffnesses a function of base size, bearing pressure, and vibration amplitude (Kim 2001). The effects of foundation shape, mass, and soil layer thickness were experimentally investigated (Ashoori 2015). Mass had a minimal effect on the dynamic response of the foundation. The shape of the foundation and layer thickness are important parameters. The embedded ratio, or the ratio of the foundation that is buried in the soil, also plays a role in the effective damping of the sand.

2.3 Cohesionless Soil Mechanics

The soil mechanics of sand and gravel was pioneered by BO Hardin in the 1960s. Hardin's seminal works include the studies of the stiffness of sand in triaxial tests (Hardin 1966), dynamic versus static stiffnesses in sand (Hardin 1965a), and the nature of damping in sand (Hardin 1965b).

Hardin and Richart conducted a series of resonant column tests on round and angular Ottawa sand and proposed that shear modulus of sand is a nonlinear function of the sand's void ratio and pressure on the sand (hardin1963). Nearly every other theory for the calculation of the moduli for

cohesionless soil since then has had been a nonlinear function of void ratio and pressure and follow the format:

$$G = A\frac{(e_g - e)^2}{(1+e)}(p)^m \quad \textbf{(1)}$$

Where *G* is the shear modulus; *A*, e_g, and *m* are constants, *e* is the material's void ratio, and *p* is pressure on the sand. Different theories use bearing, confining, mean principal pressures in these equations. Theories for the moduli of cohesionless soils found in the literature are listed in Table I.

Through a variety of testing methods including: cyclic loading, monotonic loading, resonant column test, triaxial test, torsional shear test, simple shear test, and torsional simple shear test many more theoretical equations have been proffered (Oztoprak 2013). Through comprehensive resonant column, and torsional shear test Iwasaka proposed theoretical equations with different values for *A* and *m* depending on the shear strain of the sand (Iwasaki 1977 and Iwasaki 1978). Seed et al conducted cyclic triaxial tests and offered a theoretical equation that is not explicitly a function of void ratio, but instead only an explicit function of the square root of mean principal stress. However, in the selection of the constant, *A*, parameters such as grain size, the relative density, and the shear strain of the soil need to be considered (Seed 1986). After analyzing over 100 scale model footings on sand in a centrifuge Pak and Guzina propose an equation for determining the shear modulus of sand that is very similar to Equation 1 with an added nonlinear relationship to footing radius (Pak 1995). By studying a massive database of over 50 experimental studies an equation for shear modulus is proposed that is has a simplified void ratio function, *A* and m are functions of strain and *p* is a ratio of mean principal stress over atmospheric pressure (Oztoprak 2013) (See Table I).

Attempts at micro-mechanical explanations

Characterizing damping in cohesionless soil is important to understanding its dynamic behavior. Extensive resonant-column and torsional shear tests on sand samples led Tatsuoka et al to conclude that hysteretic damp is significantly affected by strain amplitude and confining pressure. As strain increases

Table I

RELAVENT EQUATIONS FOR CALCULATING MODULI OF COHESIONLESS SOILS

Equation	Equation Number	Units	Notes	Reference
$G = 700\frac{(2.17-e)^2}{(1+e)}(p)^{0.5}$	**(2)**	Kgf/cm^2	Round Ottawa Sand, *p* is mean principal stress	Hardin 1963
$G = 326\frac{(2.97-e)^2}{(1+e)}(p)^{0.5}$	**(3)**	Kgf/cm^2	Angular Ottawa Sand, *p* is mean principal stress	Hardin 1963
$G = 900\frac{(2.17-e)^2}{(1+e)}(p)^{0.5}$	**(4)**	Kgf/cm^2	Low strain, *p* is mean principal stress	Iwasaki 1978
$G = 1000xK_2(p_m)^{0.5}$	**(5)**	Psf	K_2 is determined by soil type and character, p_m is confining pressure	Seed 1986
$G = 1.64\frac{(2.97-e)^2}{(1+e)}(Ro)^{0.1}\left(\frac{p_r}{1x10^3}\right)^{0.5}$	**(6)**	MPa	R_o is footing radius and P_r is bearing pressure	Pak 1995
$G = 5760\frac{p_a}{(1+e)^3}\left(\frac{p}{p_a}\right)^{0.49}$	**(7)**	Pa	Pa is atmospheric pressure and p is mean principal stress	Oztoprak 2013

so does damping where an increase in confining pressure reduces damping. It was also concluded that void ratio and moisture content had a small effect on damping (Tatsuoka 1978).

Other parameters have been studied for their effect on damping in sand as well. Seed found that damping ratios for sand are very similar to those for gravels and are not affected by density or particle size (Seed 1986). Ishibashi and Zhang analyzed experimental data from 15 different sources. From this they propose an equation for damping in sand that is a function of void ratio of the soil, plasticity index of the soil, and strain amplitude (Ishibashi 1993). A study of the frequency of a load also effects damping in sand. A hysteretic-viscous damping model is proposed for low frequencies while a continuum model is suggested for frequencies higher than 20 Hz (Lin 1996). The uniformity coefficient of the soil has been seen to effect damping in sand. It was observed that an increase in the uniformity coefficient, meaning an increase in the distribution of grain sizes in the sand, correlates to an increase in damping. At the same time mean grain size was not seen to affect damping in sand (Wichtmann 2012).

3 Sand as Part of Combined Vibration-Damping (CVD) Structures

3.1 Dynamic Behavior of Sand in CVD Structures

3.1.1 Experimental Data

The first step to understand the potential application of the sandbox as a vibration isolation strategy was to build a realistic model. Two experimental models were considered in this study. The first was a single CVD footing. The second was four CVD footings supporting a large steel plate.

3.1.1.1 Single-Footing Model

Frequency response data was taken of nine different configurations of sandboxes-- three sand heights and three different masses. To take this data an aluminum cylinder, or cylinders, were glued to a

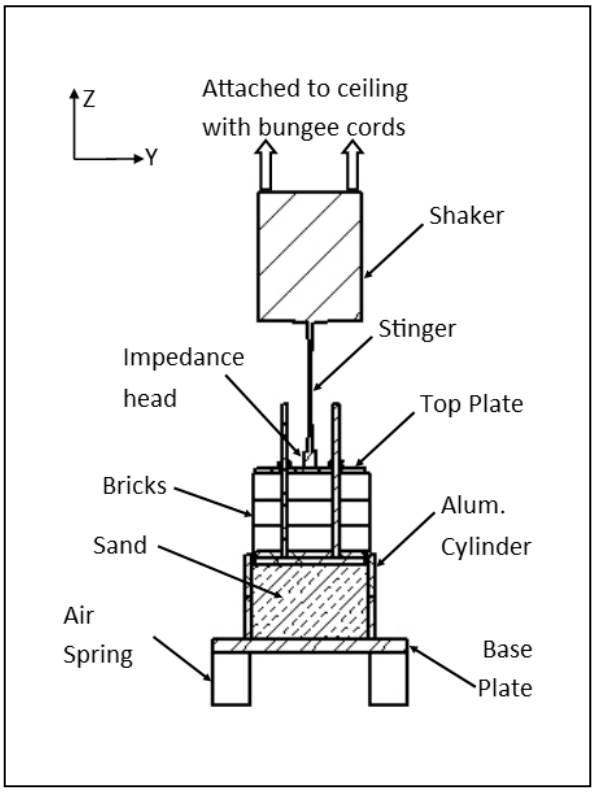

Figure 3: Experimental model of single CVD footing structure

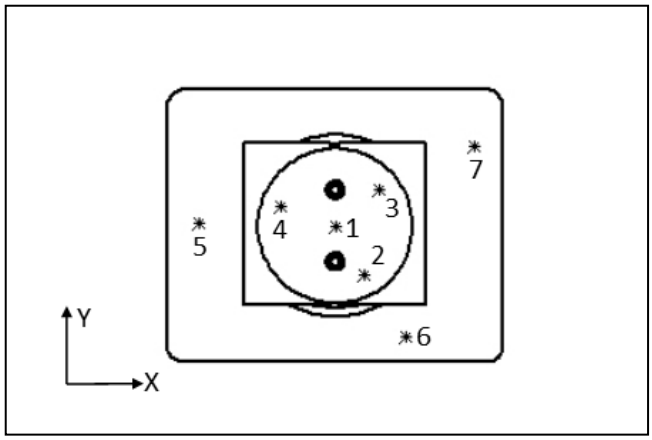

Figure 4: Vibration sensor locations on single-footing experimental model

steel plate and filled with the appropriate amount of sand--one of the three heights. On top of the sand circular, aluminum plates were loaded with lead bricks. Finally, a top plate was placed on the bricks and fastened into place with threaded rods. To isolate the sandbox test setup from the lab floor, the entire assembly was placed on air springs (Goodyear part number 1B5). A shaker (Brüel & Kjær 898890-8) was suspended by bungee cords from the ceiling and attached to the top plate via a stinger and impedance head (see Figure 3).

The shaker was connected at the center of the top plate point 1 (see Figure 4) to excite vibrational modes in the vertical direction while minimally exciting any horizontal or rocking modes. In addition to the impedance head, six piezo-based accelerometers were placed on the assembly--three on the top plate and three on the base plate (points 2 through 7 of Figure 4).

The data from the accelerometers and impedance head were collected by a Hewlett Packard (HP) E1432A 16 Channel 1.2 kSa/s Digitizer plus Digital Signal Processor with Data Physics Corporation's Signal Calc 620 Dynamic Signal Analyzer software. MatLab software was used to generate experimental force-response functions for the top and base plates.

Figure 5: Photograph of multi-footing CVD structure experimental model

3.1.1.2 Multi-Footing Model

In 2006 Curt Preissner took a set of vibration measurements on a multi-footing experimental model. This model included four CVD structures and a large steel plate. Each CVD structure consisted of a base plate, shim, square sandbox, a certain depth of sand, a square plate on top of the sand, and wedge jack. In one case studied for each footing an aluminum spacer was connected between the plate contacting the sand and the wedge jack. Between the base plate and the shim, and between the shim and the sandbox a layer of 3M™ vibration damping tape was placed. The top plate was a 1.8 m x 1.2 m x 0.1 m steel plate. The plate was place on top of the four footings spaced in a rectangle of 1.1 m x 1.0 m. The center of mass was of the plate was placed in the center of the rectangularly spaced footings (see Figure 5).

Accelerometer measurements were taken on the top plate at points directly above the 4 legs and at the center of the place and on the ground next to the footings. Ambient vibration measurements were taken in the X-, Y-, and Z-directions. An additional set of measurements were taken in the Z-

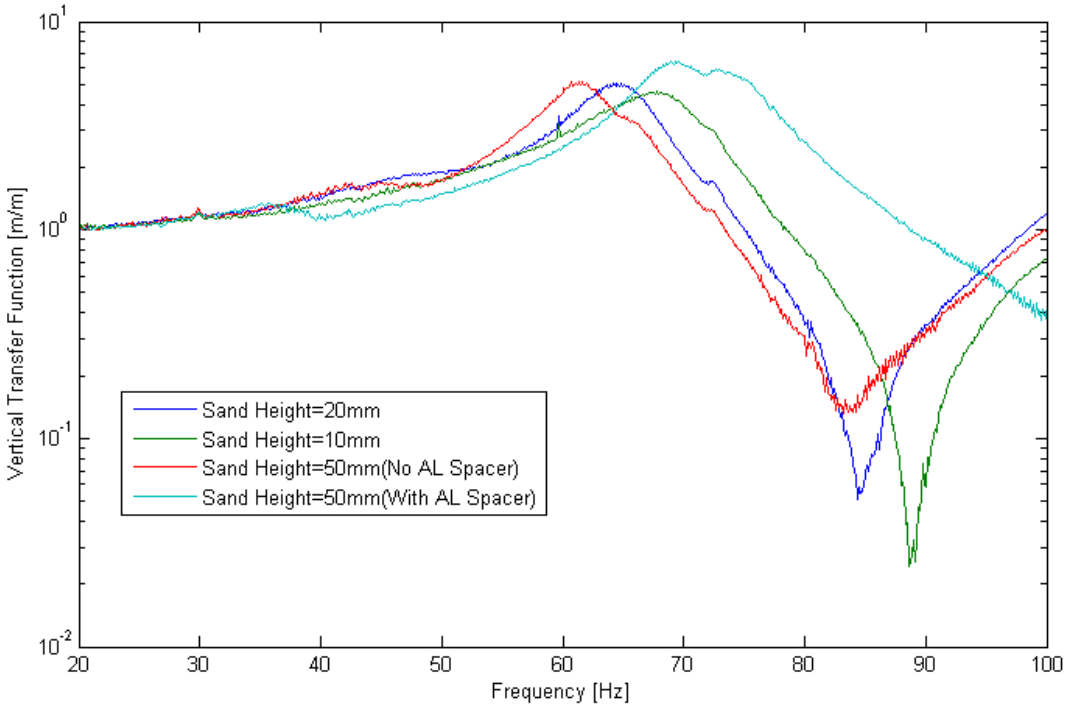

Figure 6: Experimental transfer functions for the multi-footing model in the vertical direction with shaker adding vibrational energy

direction. In these cases, the B&K shaker was placed on the ground and produced random chirps to add more vibrational energy to the system. The data was recorded by an HP35668 two-channel analyzer. The analyzer produced power spectra data as well as transfer function data of the plate over the floor. MatLab software was used to further analyze the transfer function data. Figure 6 shows the transfer functions in the vertical direction of the experimental cases studied in which the B&K shaker was adding vibrational energy.

3.1.2 2 Degree-of-Freedom Analytical Model

Using the single-footing model with the force from the shaker centered (point 1 of figure 4), an analytical model of the 2 degree-of-freedom system was built. Figure 7 shows the block diagram of the model of the single-footing sandbox test setups. The bricks, threaded rods, and aluminum plates are the

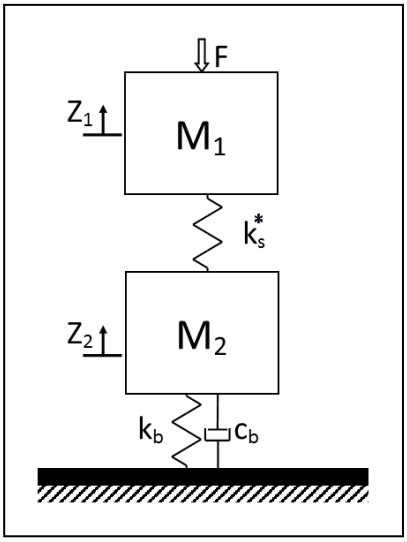

Figure 7: Block diagram of 2 degree-of-freedom analytical model of the single-footing experimental model

top mass (M_1) connected to the base plate (steel plate) and cylinder(s) (M_2) by a spring, k_s^*. The spring has a real and imaginary part k_s and k_{si}, respectively. If η is k_s/k_{si} the final expression is $k_s^*=k_s(1+i\,\eta)$. The bottom mass is connected to the "rigid" lab floor by a spring-damper representing the air springs (k_b, c_b).

Equation 8 shows the frequency response functions for the 2 degree-of-freedom system in the frequency domain:

$$\begin{bmatrix} Z_1/_F \\ Z_2/_F \end{bmatrix} = \begin{bmatrix} -\omega^2 M_1 + k_s(1+i\eta) & -k_s(1+i\eta) \\ -k_s(1+i\eta) & -\omega^2 M_2 - i\omega c_b + k_s(1+i\eta) + k_b \end{bmatrix}^{-1} \begin{bmatrix} 1 \\ 0 \end{bmatrix} \quad \textbf{(8)}$$

The masses of all components were measured. Therefore, four variables need to be determined—air spring and sand stiffness and damping (k_b, k_s, c_b, and η)—to complete the model.

3.1.2.1 Properties of Air Springs

Air spring effective stiffness and damping were determined by placing only the base plate on the air springs and striking it with an impact hammer (Brüel & Kjær 8202) in the center of the plate.

Assuming a single degree-of-freedom system, damped natural frequency (ω_d) and quality factor (Q) are easily obtained from the frequency-response data. With these two quantities and the mass of the base plate (M_p), effective air spring stiffness (k_b), and damping (c_b) were solved for from the following equations:

$$\omega_d = \sqrt{\frac{k_b}{M_p}(1-\zeta^2)}, \zeta = \frac{1}{2Q} = \frac{c_b}{2\sqrt{k_b M_p}} \quad \textbf{(9,10)}$$

The effective air spring stiffness and damping were determined to be k_b =187 kN/m and c_b =276 Ns/m, respectively.

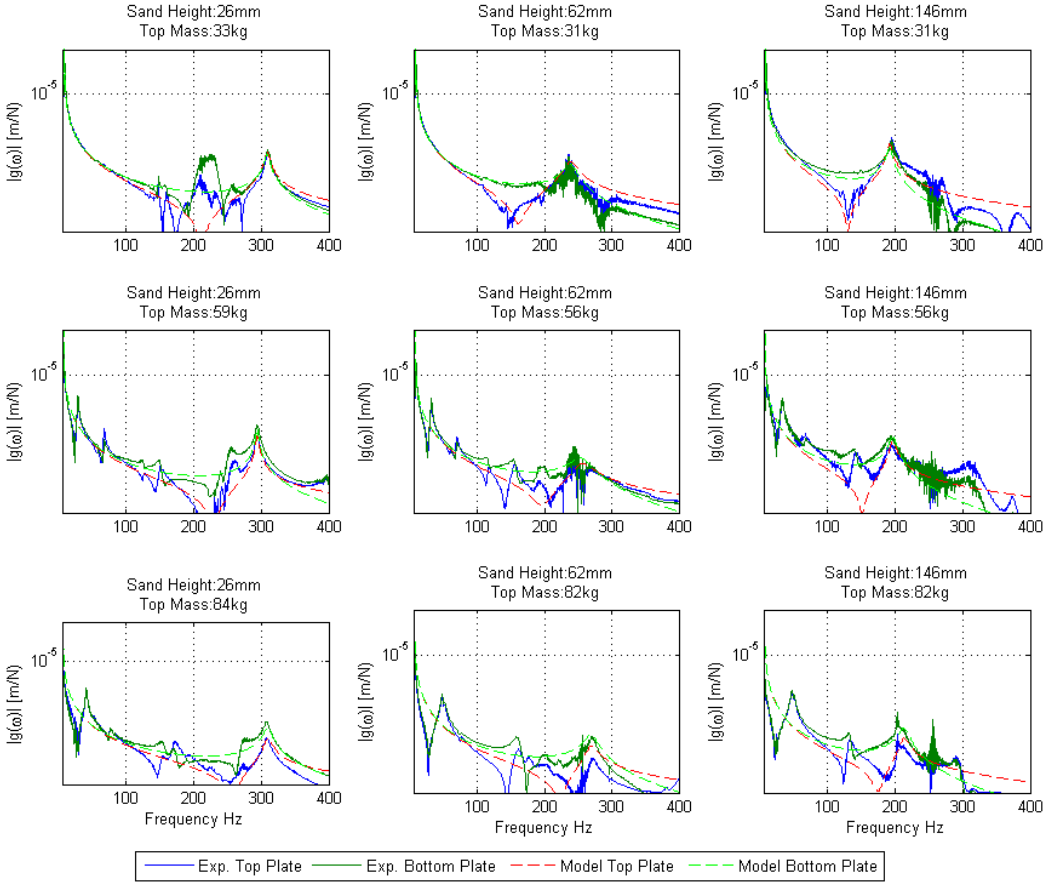

Figure 8: Experimental and modeled force-response-functions of the top and bottom plates of the single-footing model

3.1.2.2 Dynamic Properties of Sand

Values of k_s and η in the model (Equation 8) were varied. The combination that produced the lowest squared error between the model and the experimental data was used for the stiffness and damping values. Modeled force response data and corresponding k_s and η values were obtained for all nine test setups. Figure 8 shows the experimental and analytical model force-response-functions with k_s and η optimized for each test setup.

The optimized analytical model predicts two distinct peaks for each of the nine experimental model setups. The first in all setups is located between 5 and 10 Hz. This is the base plate moving in phase with the top mass (M_2 and M_1, respectively). The second peak higher in the frequency range is the resonance of M_1 and M_2 moving out of phase with each other. The sand height is the most important parameter in determining the resonance location. So, for low sand heights (26 mm) the second peak is located around 300 Hz, for medium sand heights (62 mm) the second peak is from 240 to 260 Hz, for high sand heights (146 mm) it's right around 200 Hz.

There are other resonant peaks seen between the two predicted from the analytical model in the medium and heavy (59 and 84 kg) setups. These peaks seen in the experimental data are most likely rocking or swaying modes in the experiment that were excited because the shaker was not perfectly aligned with the center of mass. It makes sense that they would appear in heavier setup because adding bricks to add mass also adds height to the experimental model and thus amplifying the effect of an off centered load.

Gazetas (1983) proposed a formula for vertical stiffness of rigid circular foundation on a stratum-over-rigid-base:

$$k_v = \frac{4GR}{1-\nu}\left(1 + 1.28\frac{R}{H}\right) \textbf{ (11)}$$

For the sandbox footings *G* is the shear modulus of sand, *R* is the radius of the contact plate on the sand, and *H* is the sand height. From Equation 11 and the values determined for stiffness from the analytical model shear moduli (G_s) for each setup were calculated.

$$E = 2G(1 + \nu) \textbf{ (12)}$$

Equation 12 was used to convert the shear moduli obtained from Equation 11 into Young's modulus for each setup (see Table II).

TABLE II

CALCULATED YOUNG'S MODULUS AND DAMPING FROM SINGLE-FOOTING EXPERIMENTAL DATA

Top Mass M_1 [kg]	Sand Height h_s [mm]	Young's Modulus E [MPa]	Damping η
33	26	45.1	2.0×10^{-2}
	62	52.1	6.8×10^{-2}
	146	59.8	2.9×10^{-2}
59	26	52.7	1.1×10^{-2}
	62	78.2	10.4×10^{-2}
	146	81.1	3.6×10^{-2}
84	26	66.4	2.9×10^{-2}
	62	99.1	5.9×10^{-2}
	146	108.6	5.6×10^{-2}

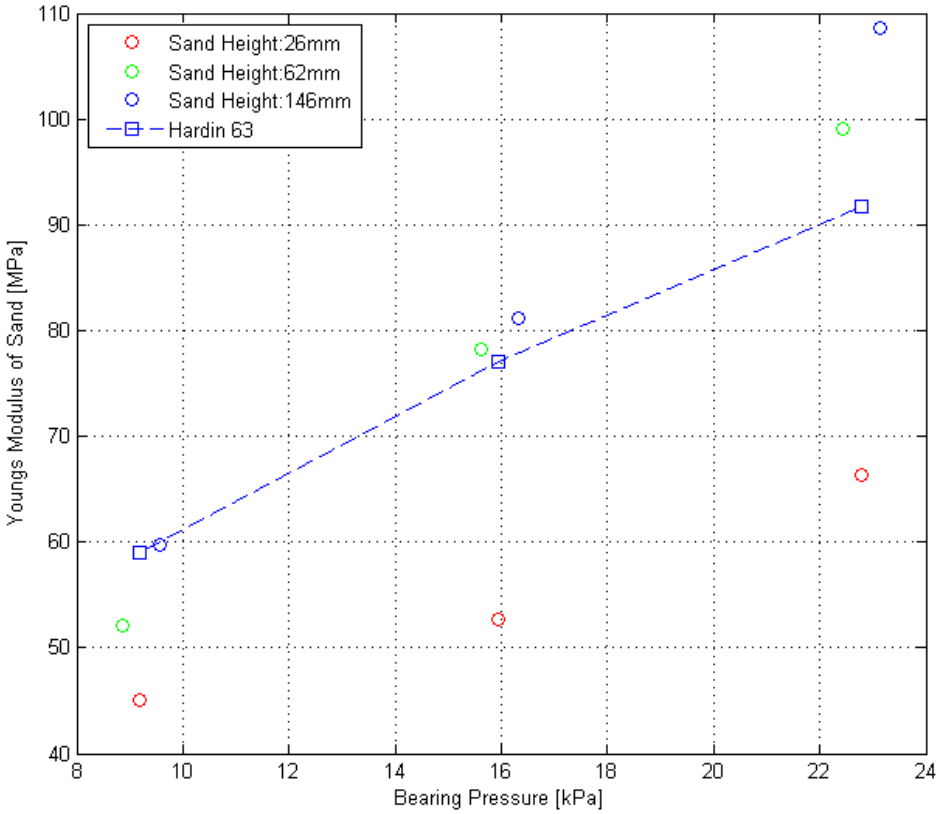

Figure 9: Experimental and theoretical values for Young's modulus versus bearing pressure

Pressure on the sand has been shown to be a factor in the determination of dynamic moduli (Hardin 1963, Pak and Guzina 1995, Iwasaki 1977, Seed 1986, Iwasaki 1978, Oztoprak 2013, Al-Homoud 1996). This was also observed in the experimental data taken.

Void ratio and Poisson's ratio were assumed to be 0.70 and 0.33, respectively , which is consistent with the literature (Al-Homoud 1996 and Das 2013). the best fit for the experimental data was Equation 2 proposed by Hardin and Richart (see Table I). The result is in units of kilogram-force per square centimeter. Where *e* is the sand's void ratio and *p* is the mean principal stress in kgf/cm^2. The mean principal stress is calculated from the following equation*:* $p=(P_r+2*P_m)/3$. Here P_r is bearing pressure and P_m is confining pressure. Confining pressure was calculated from bearing pressure:

$P_m=P_r v/(1-v)$. In this equation it is assumed there is no strain in the sleeve (aluminum cylinder or box). The Young's modulus for aluminum is much larger than that of the sand samples studied here, so this assumption is valid.

Using Equation 2 the shear moduli of sand for each experimental setup was calculated. After converting the modulus into SI units Equation 12 yielded the Young's modulus. Figure 9 shows the calculated Young's moduli of each experimental setup seen in Table II and the calculated Young's moduli from Equations 5 and 6 versus bearing pressure.

3.1.3 Finite Element Models

A 3-dimensional finite element model was created with Comsol Multiphysics software. This was done for both the single- and the multi-footing experimental models.

For all aluminum, steel, and lead components of both models the material properties were selected from the "built in" options in the software. The sand Young's modulus, Poisson's ratio, and density needed to be inputted. Equations 5 and 6 were used to determine the Young's modulus of the sand for each experimental setup being simulated. Poisson's ratio was selected to be 0.33. The mass of

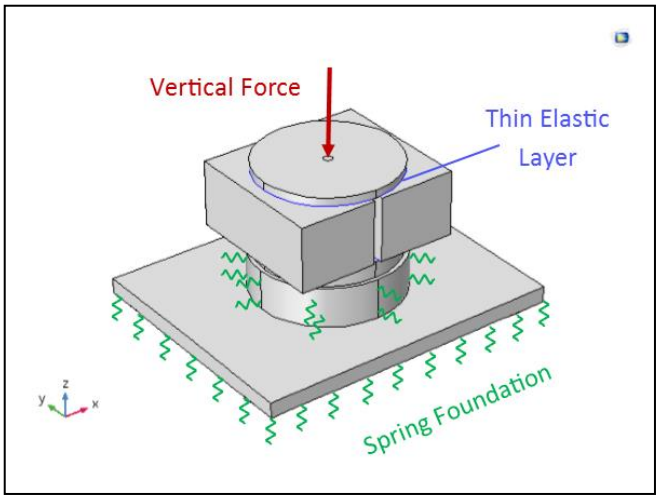

Figure 10: Finite element model of single-footing model in Comsol Multiphysics

the sand for each sand height of the experimental setup was measured. With this, the density of the sand was easily determined as: ρ_s=1560 kg/m3.

The “build union” option was used to create a “bonded” connection between components of the assembly. Boundary conditions for the sand had to be carefully selected. The simple “union” condition used for the rest of the model would not produce desirable results because sand is a granular material not a solid. Sand can only support compressive and shear stresses not tensile stresses. A different approach was needed to model these boundary conditions for the single- than the multi-footing model. This is because for the single-footing model the sand is enclosed in a cylinder and for the multi-footing model the sand is enclosed in a square box.

Mesh size also proved to be important to accurately simulate the sandbox experiments. This is most important for the sand because it is subject to the most deformation. A maximum triangle element size of 0.0064 m gave was used to mesh the top surface of the sand. This maximum element size was chosen to be this size because that is the difference between the contact plate radius and the inner diameter of the cylinder. If the maximum element size is set larger than 0.0064 m there is a divergence in the results of the simulation. If the maximum elements size is set smaller there is no divergence, but the computation time is longer.

3.1.3.1 Single-Footing Model

For simplicity the threaded rods, nuts and washers were omitted from the 3D model.

To model the damping in sand a damping node was added to the solid mechanics section of Comsol. Loss factor damping was selected for the damping type. The mean value of η for the sand from all nine setups is $\eta=4.6\text{x}10^{-2}$ was used for all simulated test setups

To simulate the aluminum cylinder/sand interface a “spring foundation” was added to the sand at the interface location while omitting the aluminum cylinder. The spring value was set to zero in the vertical direction. Constraining the vertical motion of the sand/cylinder interface would create

unrealistic tensile stresses in the sand. The horizontal spring values were calculated from the stress-strain relationship for a cylinder. The expanding sand causes hoop stresses in the cylinder. The hoop stress for a cylinder is: $\sigma_\theta = \frac{Pr}{t}$, where *P* is pressure, *r* is the radius of the cylinder, and *t* is the thickness of the cylinder. Using Hooke's law and the fact that strain in the θ-direction reduces to the change in radius of the cylinder we have: $\frac{\mathrm{Pr}}{\mathrm{t}} = \frac{\mathrm{E}\Delta\mathrm{r}}{\mathrm{r}}$, here *E* is Young's modulus of aluminum. The previous equation was then rearranged to solve for spring constant per unit area: $\frac{\mathrm{k}}{\mathrm{A}} = \frac{\mathrm{f}\Delta\mathrm{r}}{\mathrm{A}} = \frac{\mathrm{Et}}{\mathrm{r}^2}$. Using the values E=6.9x10^{10} Pa, t=0.0127 m, r=0.1143 m the spring constant per unit area was determined to be: kA=6.71x10^{10} N/m/m^2. This number was used for the horizontal spring foundation values.

To simulate the air springs a "spring foundation" was used on the base plate (see Figure 10). The value determined for the effective air spring stiffness (k_b=187 kN/m) was used as the total spring force of the spring foundation. The Damping value c_b was not included in the FE simulation. The low damping value meant it will not substantially change the results but adding damping to the simulation does increase computation time.

A vertical force was with an amplitude of 1 N was applied to the center of the top plate to simulate the shaker force. The "Frequency Domain" study calculates the response of the model to a harmonic force—in this case, the single vertical force—at a desired set of frequencies. The force magnitude of 1 N was chosen so that plotting of the top and base plate displacements by frequency is the same as the displacement force-response-functions generated by the experimental data and the analytical model.

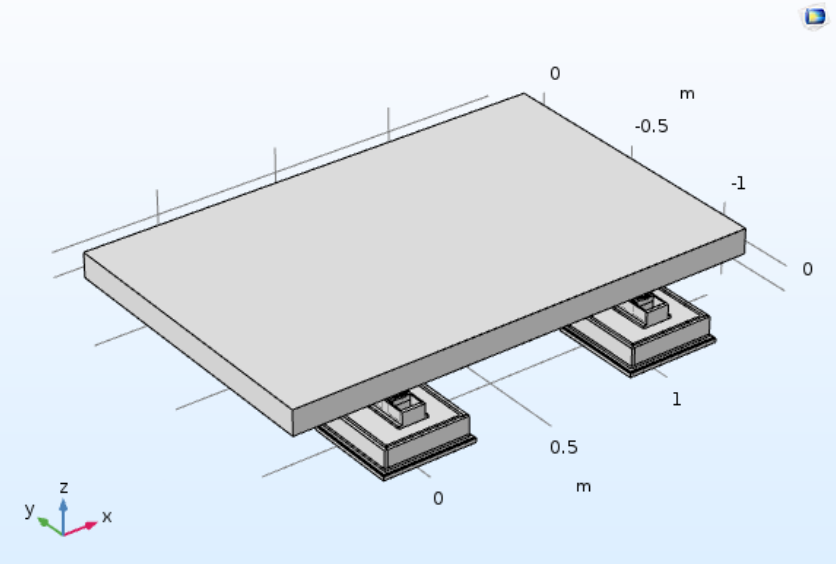

Figure 11: Multi-footing finite element model in Comsol Multiphysics

3.1.3.2 Multi-Footing Model

A simplified model of the multi-footing model was imported into Comsol. To simulate the sand/aluminum sandbox interface a "thin elastic layer" was placed at the contact surfaces between the sand and the vertical walls of the sandbox (see Figure 11). The horizontal stiffnesses were set very high (10^{20} N/m/m^2) to simulate a near bounded contact between the sand and the sandbox. In the vertical direction the stiffness of the thin elastic layer was set to 0. This was so unrealistic tensile stresses at the sand/sandbox boundary were not created in the sand.

It is clear from the experimental transfer function data that there is a resonance in the vertical direction (see Figure 6). It was assumed this was the vertical resonance in a single degree-of-freedom system. From this it is easy to determine the equivalent stiffness of the four footings together. Assuming that the footings have equal stiffness then Equations 11 and 12 can be used to determine the Young's modulus of the sand in the experimental CVD.

In the same way that the air spring damping was calculated in section 2.1.2.1, Equation 10 was used with the experimental data to determine damping. Table III shows values of Young's Modulus and damping calculated from the experimental data.

TABLE III

CALCULATED YOUNG'S MODULUS AND DAMPING FROM MULTI-FOOTING EXPERIMENTAL DATA

Top Mass M_1 **[kg]**	**Sand Height** h_s **[mm]**	**Young's Modulus E [MPa]**	**Damping** η
1405	10	7.7	9.1×10^{-2}
1405	20	13.2	13×10^{-2}
1405	50	26.0	10.2×10^{-2}
1510	50	36.5	11×10^{-2}

The values for Young's modulus best fit the theory proposed by Pak and Guzina, Equation 6 (Pak 1995). Effective footing radius can be calculated from the area of the footing as following: $R_o = \sqrt{\frac{A_f}{\pi}}$. Figure 12 shows the calculated Young's moduli of each experimental setup seen in Table III and the calculated Young's moduli using Equations 6 and 12 versus bearing pressure.

Again, the "Frequency Domain" study was used to simulate the transfer function results produced from the experimental data. However, a force on 1 N was not used in this case. Instead, the bottom of the four footings were set to a "prescribed displacement." To obtain the transfer function the

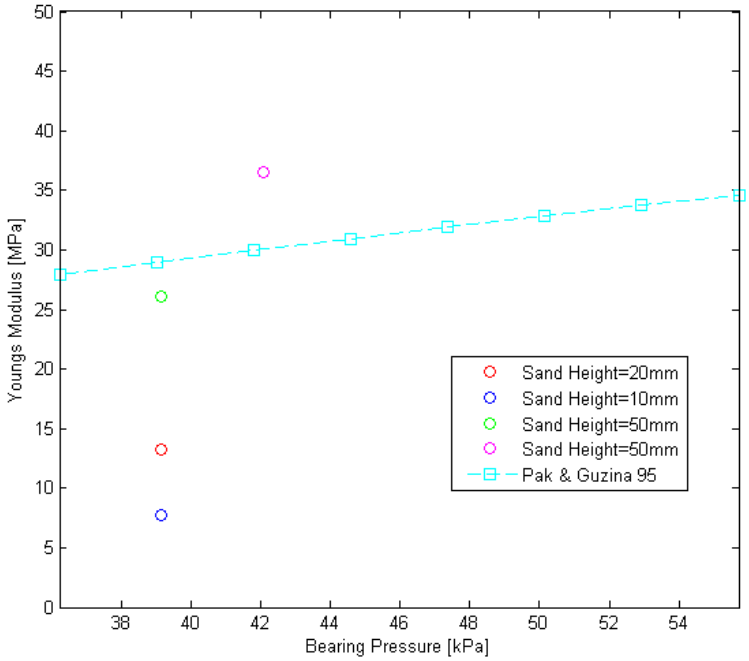

Figure 12: Experimental and theoretical values of Young's modulus versus bearing pressure

displacement measured on the table is divided by the prescribed displacement. Displacement was prescribed in the X-, Y-, and Z-directions to simulate the experimental transfer functions.

The Young's Moduli calculated from Equations 6 and 12 were used in the FEM as well as ν=0.33 and ρ=1560 kg/m^3. The mean value of the calculated damping, η=11x10^{-2}, was used as the loss factor in all simulations.

3.1.4 Results

3.1.4.1 Single-Footing Model

Figure 13 shows the experimental data, the experimentally based analytical model, and FE model results for all nine sandbox configurations. The analytical model uses stiffness derived from G_s

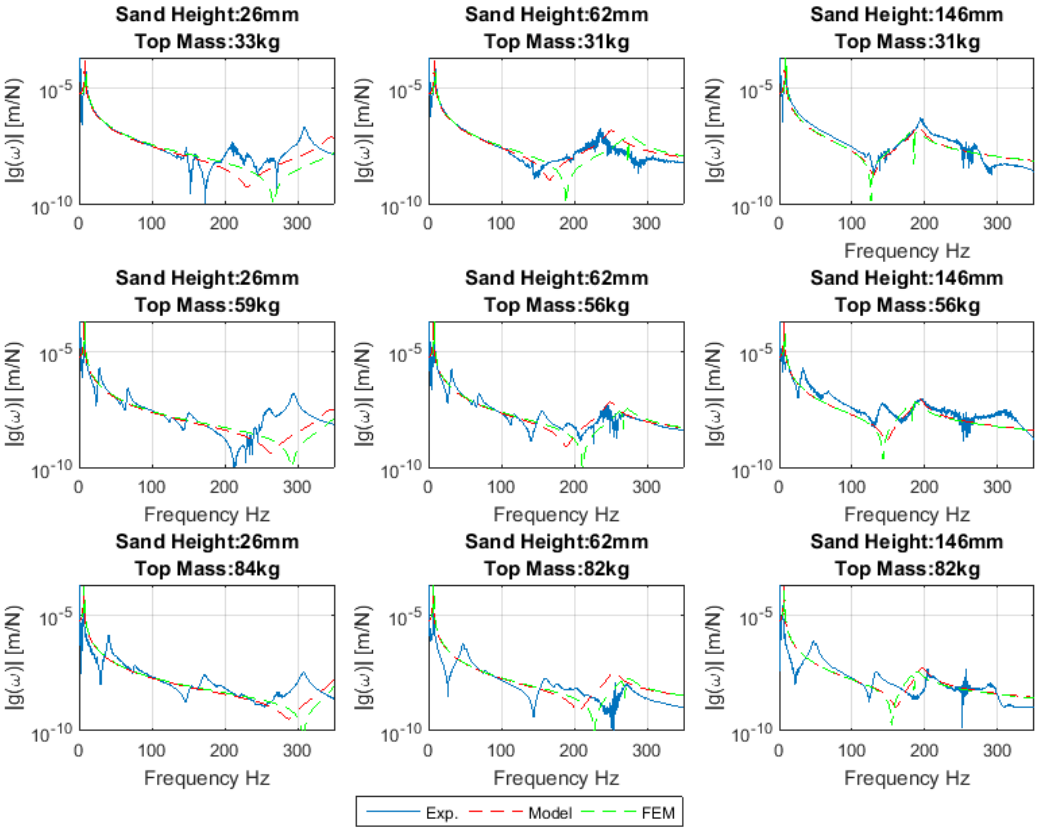

Figure 13: Force-response-functions from experimental, analytical, and FE models of single-footing top plate

using Equations 11 and 12. The FE and analytical models give similar, but not identical results. Both models accurately predict two resonances seen in the experimental data for medium (62 mm) and high (146 mm) sand heights.

For the rest of the other resonant peaks seen in the experimental data these most likely represent rocking or swaying modes in the experiment that were excited because the shaker was not perfectly aligned with the center of mass. Furthermore, it is unlikely that each of the four air springs had identical stiffness. This could be due to them being filled or loaded unevenly. This would further exaggerate rocking modes.

For the low (26 mm) sand height, both the analytical and the FE models do not accurately predict the location of the second resonant peak at around 300 Hz. The analytical model of the low top mass (31 kg) and low sand setup comes close to capturing that peak accurately. However, for the rest of the low sand models the second resonance peak is missed by up to 50 Hz. This is most likely due to shunting. As the sand stiffness increases as a function of sand height components previously assumed to be rigid in the models can no longer be assumed as such.

In the experimental model the most likely components that could no longer be considered rigid were the threaded rods that sandwich the lead bricks between the top plate and lower cylindrical plates. The FEM was modified to take into account nonrigid rods. The stiffness of the rods was modeled as $\mathrm{k_r} = \frac{\mathrm{AE}}{\mathrm{L}}$. A "thin elastic layer" was placed between the top plate and bricks interface surfaces with k_r as the stiffness connecting plate and bricks. Figure 14 shows the FE simulation and experimental data for low sand configurations. It is seen that the resonance peak at around 300 Hz is predicted by the FE model.

Most of the experimental data show more than two resonant peaks. One of these peaks can be captured in the models by assuming air spring stiffness is also a function of mass. Figure 14 shows the FE simulation results predicting new first resonant peak locations. The stiffness of the air springs is not further investigated because varying air spring stiffness does not affect sand stiffness (the main focus of this investigation) to any significant extent.

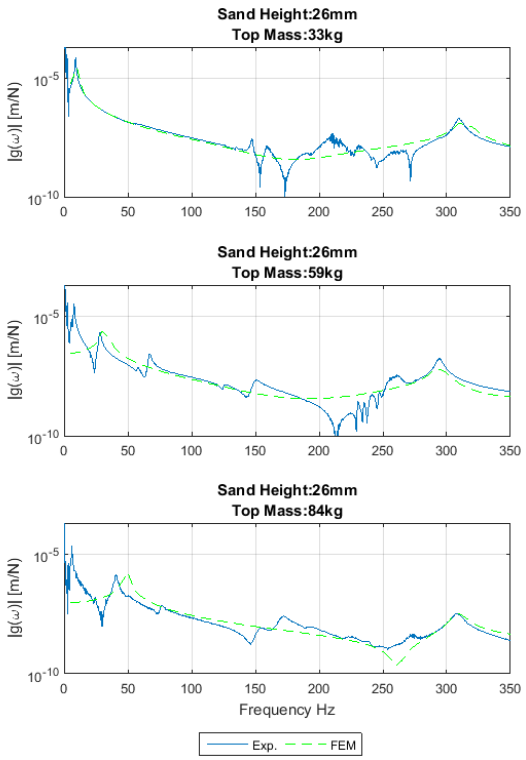

Figure 14: Experimental and FE modeled force-response-functions with compliant threaded rods and varied air spring stiffness

3.1.4.2 Multi-Footing Model

Like the single-footing model, the theoretically predicted Young's modulus is higher than the moduli calculated from the experimental data for the CVD structures with low sand (10 and 20 mm). Shunting is most likely the issue again. For the FEM simulations in these cases the calculated stiffness of the bolts connecting the wedge jack to the sand contact plate were added by a “thin elastic layer.” This allowed the FEM data to correlate more closely to the experimental data.

Figures 15 and 16 shows the experimental and FE model transfer functions in the X-, Y-, and Z-directions of the four cases studied. The FE model predicts the resonances in all three directions and matches the damping seen. Considering that Young’s modulus was calculated from the vertical (Z-direction) data this is a good result. Even considering shunting in the 10 mm sand height CVD structures

the modeled resonance peaks are still higher than the experimental measurements. There is, probably, more shunting to be accounted for, but the result is good for our purposes.

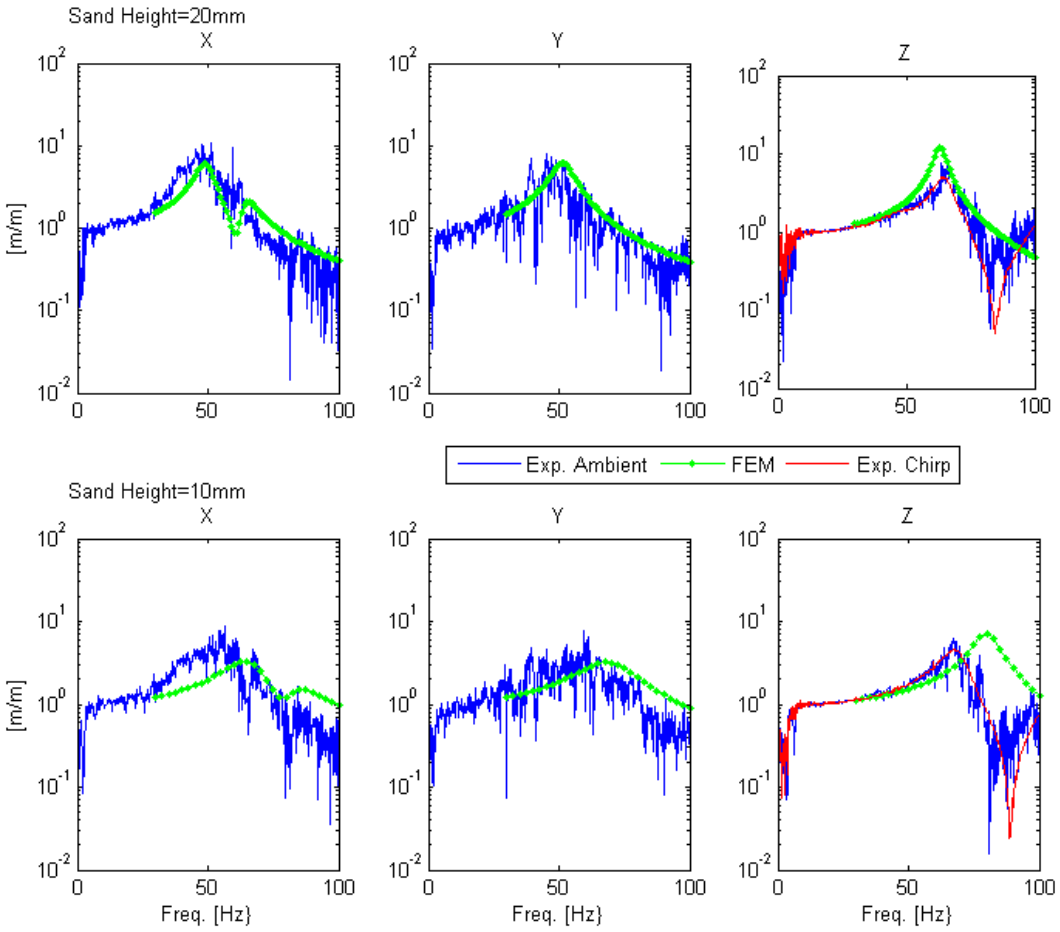

Figure 15: Experimental and FE modeled multi-footing transfer functions in the X-, Y-, and Z-directions for sand heights of 20 and 10 mm

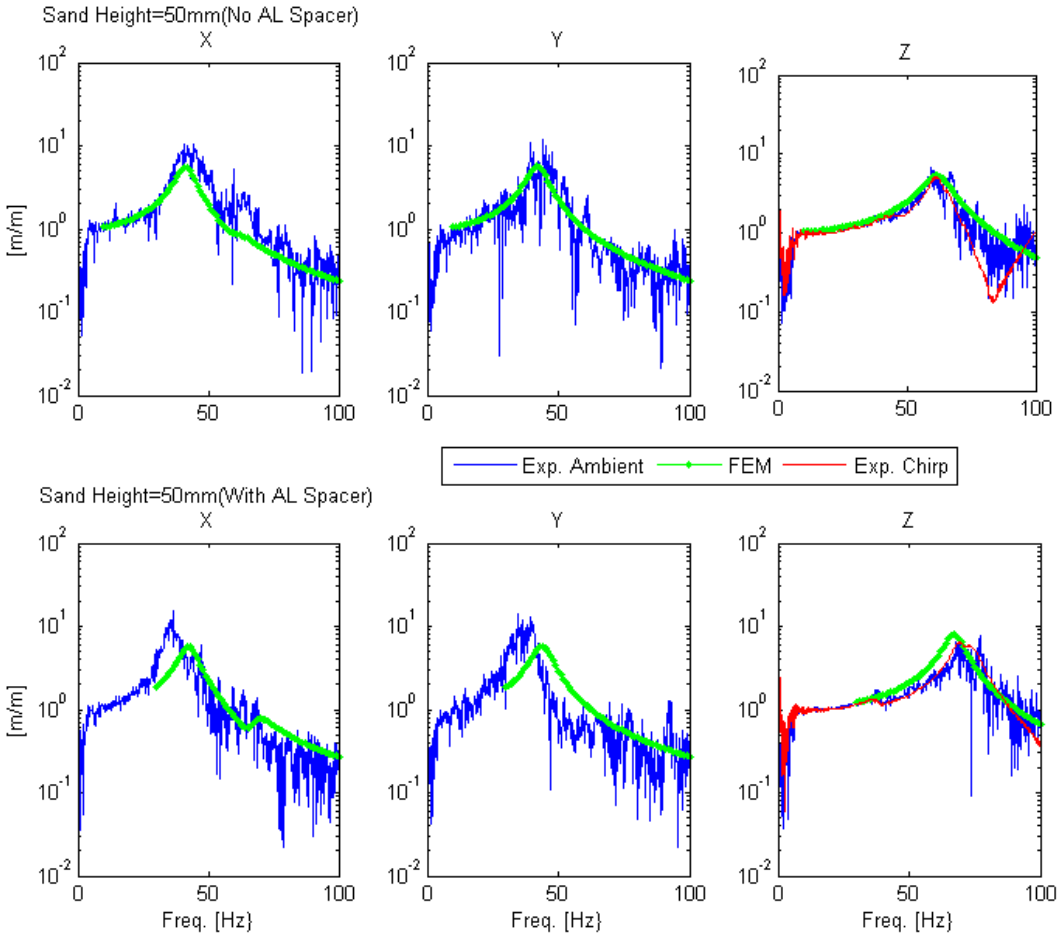

Figure 16: Experimental and FE modeled multi-footing transfer functions in the X-, Y-, and Z-directions for sand heights of 50 mm with and without aluminum spacers

3.2 Design of Future Combined Vibration-Damping Structures

3.2.1 Objectives

The environmental noise in the experiment hall at the APS has been studied (Anton 2016 and Kearney 2016). These studies have shown that noise from mechanical equipment is added to the experimental hall floor in the 10 to 60 Hz range.

The goal was to design CVD footing structures that produce instrument tables with resonant frequencies furthest away from vibrational energy around 30 Hz and 60 Hz.

One way to achieve this is to have resonant frequencies low enough to attenuate higher frequency noise. Damping has to be large enough so that low frequency vibrations are not amplified to an unacceptable level. The problem with this is that any change in parameters that decrease natural frequencies also lower damping.

The other way is to move the resonant frequency out of the range of vibrational energy added from mechanical equipment. This will increase damping but will not attenuate noise at lower frequencies.

The data taken from the APS experiment hall can be combined with FEM simulated transfer functions to get predicted noise levels on the table top. The NIST-A criterion for vibrational noise was used as a guide in designing the CVD structures. As described above, the NIST-A criterion calls for vibration levels to be below a constant rms displacement of 25 nm from 1 Hz to 20 Hz and below a constant rms velocity of 3.1 μm/s from 20 Hz to 100 Hz. The criterion displays noise levels in a standard proportional bandwidth (one-third octaves).

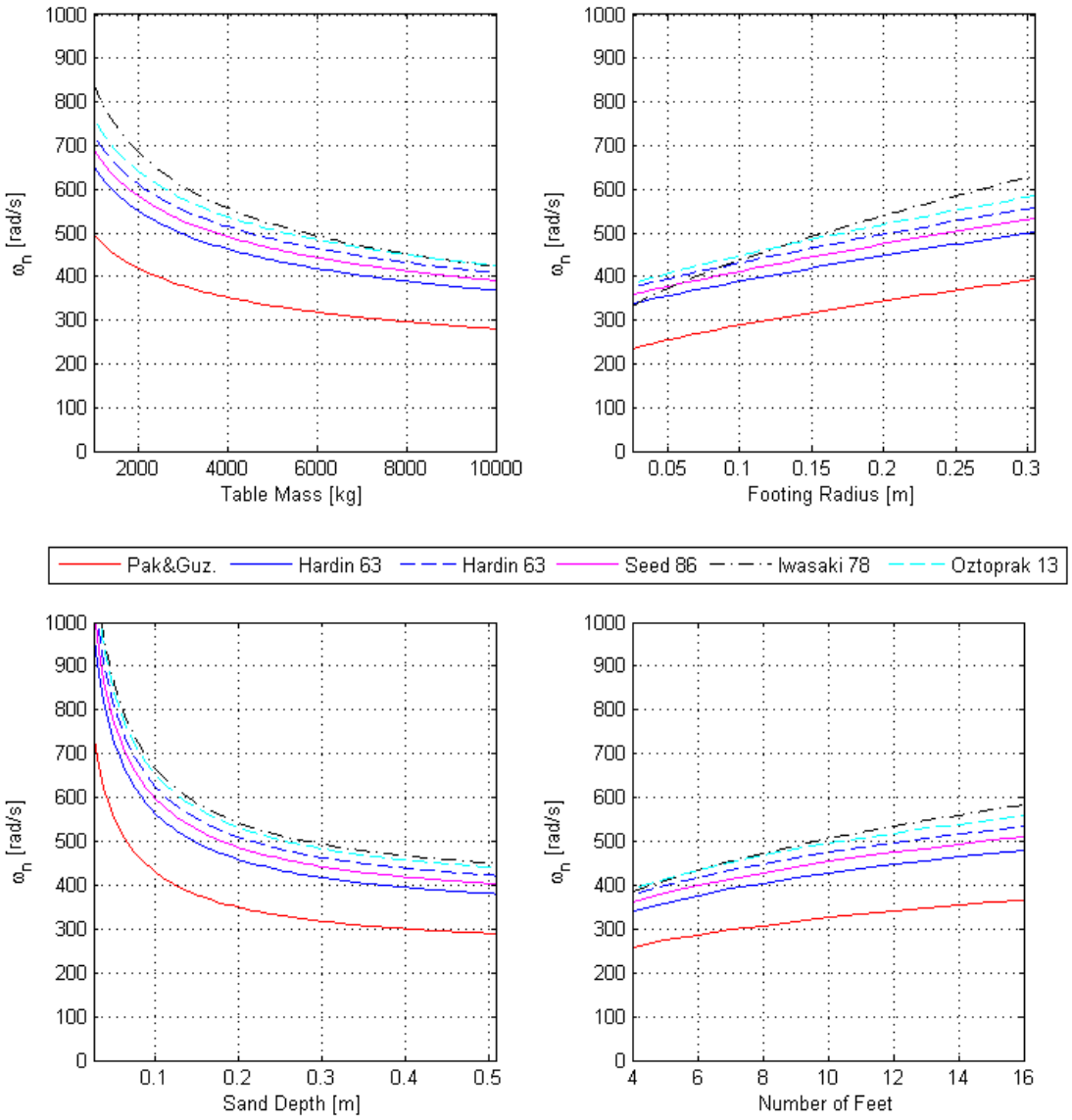

Figure 17: Parametric study of CVD footings from theoretical equations in Table II

3.2.2 Parametric Study

Figure 17 shows a parametric study of calculated values for vertical natural frequency. The stiffnesses were calculated the equations in Table I for shear modulus in combination with Equation 4. Assuming a single degree-of-freedom system, vertical natural frequencies were calculated. The

parameters chosen to study were mass (m), footing radius (r), sand depth (h_s), and number of footings used (n_f).

As expected, mass is inversely related to natural frequency. However, because shear modulus increases with bearing pressure, and in this case mass increases bearing pressure, stiffness also increases with mass. The natural frequency is proportional to $1/m^{0.25}$. Sand height is also inversely related to natural frequencies with a relationship of $1/h^{0.5}$.

Footing radius and the number of footings does increase the natural frequency despite lowering bearing pressure, all other things being equal. For footing radius, this is because the stiffness equation (Equation 11) has an r^2 term in it. While the number of footings proportionally lowers the bearing pressure, the shear modulus is only affected at $P^{0.5}$ (see Equations 2 through 8 in Table I). The effective

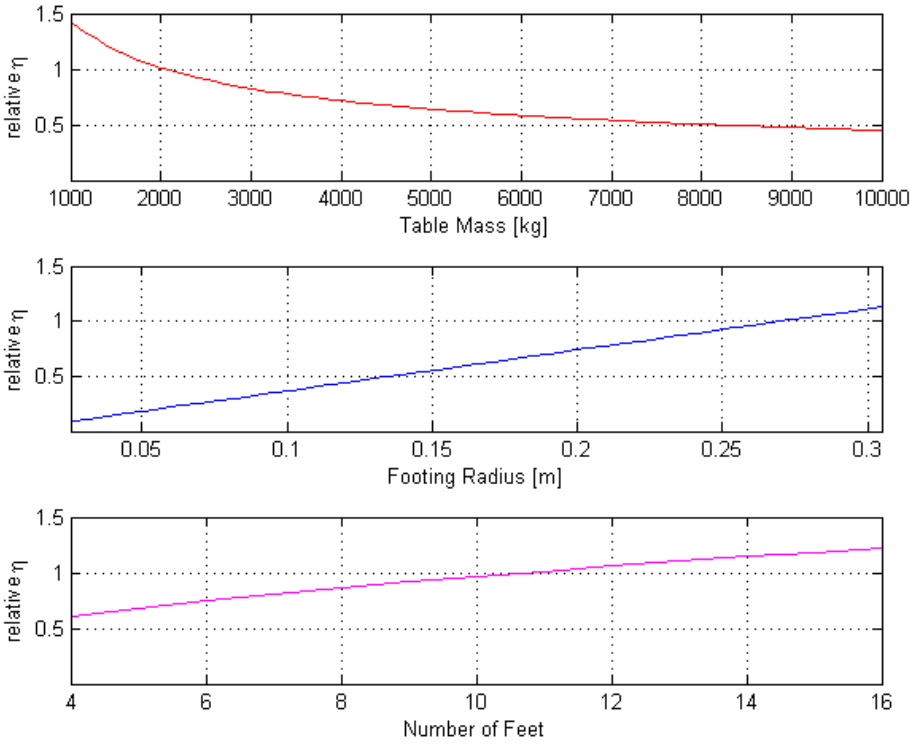

Figure 18: Parametric study of damping factor

stiffness of the system is proportional to the number of footings. This results in natural frequencies being proportional to $n_f^{0.25}$.

A parametric study of damping was also conducted. The literature suggests that damping is inversely proportional to the square root of the pressure on the sand (Tatsouka 1978). This was not seen in the experimental data taken for the single- or multi-footing experimental models. This is most likely due to the limited range of pressures on the sand. However, when designing these structures for application at the APS a large pressure range will have to be considered. Figure 18 shows the effect each parameter has on damping. These are not exact results but relative values for η if each parameter were changed. The η is proportional to $1/m^{0.5}$, r, and $n_f^{0.5}$.

3.2.3 Results

A granite instrumentation table similar to ones used at the APS was created in Comsol. The mass of the table is 9300 kg. If the same, or very similar, sand as what was used in the multi-footing experimental model Young's modulus can be determined from Equations 6 and 12. Since damping is inversely proportional to $p^{0.5}$ damping for the sand was calculated as:

$$\eta_2 = \eta_1 \sqrt{\frac{p_1}{p_2}} \textbf{(13)}.$$

Where η_1 is the damping used in the multi-footing models (11×10^{-2}) and p_1 is the mean principal stress on the sand (25 MPa). The mean principal stress calculated for the FEM table and CVD assembly is p_2. And η_2 is the damping used for the sand in the FEM.

In the first simulation an attempt was made to minimize resonant frequencies while maintaining a high enough level of damping. For this simulation the sand height was 1.0 m, the footing radii were 0.32 m, and 3 footings were used. The calculated values for Young's modulus and damping were E=114 MPa and η_2=0.087.

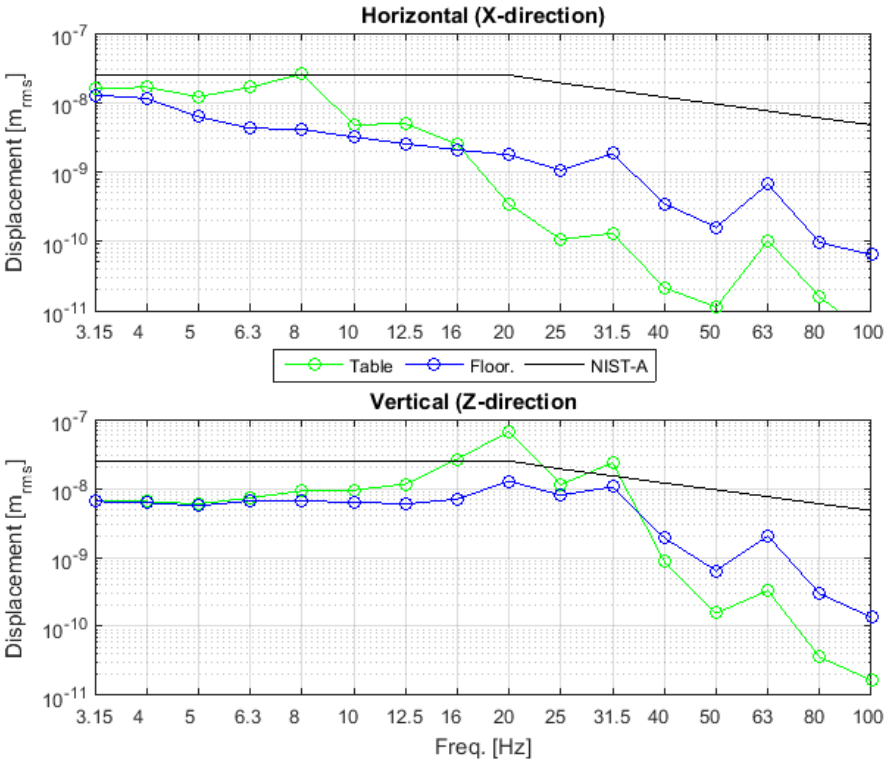

Figure 19: Measured floor and predicted table vibrations with low natural frequencies in 1/3 octave bands

For the second simulation it was attempted to make damping as high as possible and move the resonant frequencies higher than most of the vibrational energy present at the floor. To maximize damping bearing pressure was minimized this was accomplished by removing all footings and placing the entire table on top of a layer of sand. The sand height was 0.10 m, the calculated Young's modulus was E=61 MPa and the damping was eta=0.15.

Transfer functions were created for the X-, and Z-directions in the same way as explained for the multi-footing FEM in section 2.1.3.2. Transfer functions were created for the average displacement on the table top. Therefore, points nearer the center of the table will have lower displacement while points nearer the edge will have high displacement. The resulting transfer functions were multiplied by the vibration measurements taken on the floor of the APS experiment hall. Figures 19 and 20 show the

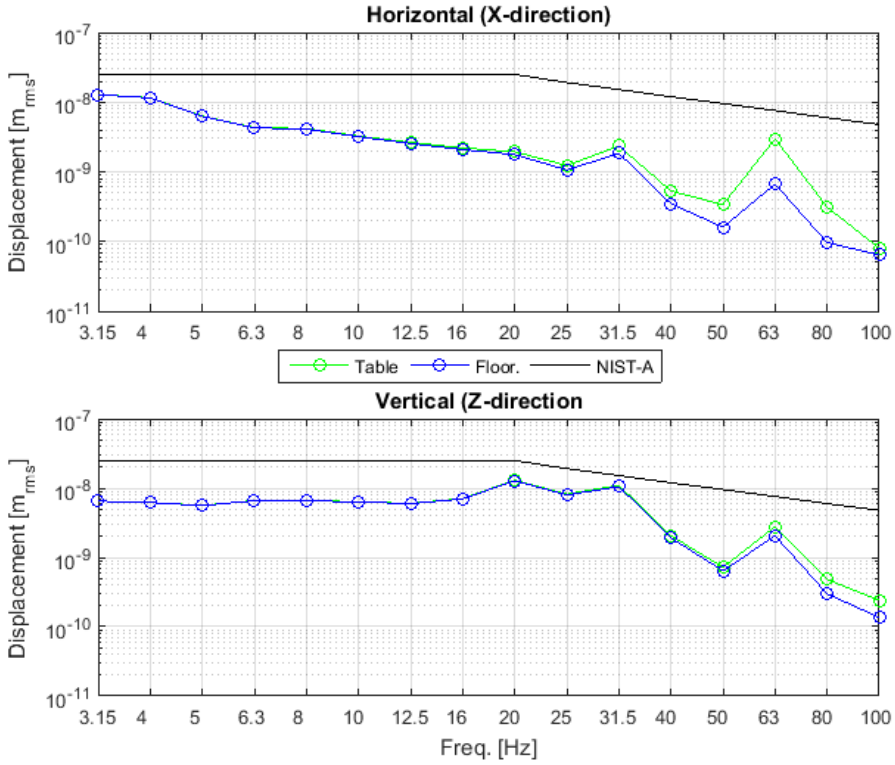

Figure 20: Measured floor and predicted table vibrations with high natural frequencies in 1/3 octave bands

measured floor vibrations, the predicted table vibration, and the NIST-A criterion for both simulations and in the X- and Z-directions.

It is seen in the first simulation that the table with the CVD structures amplify the vertical vibrational energy from the floor the most at the 20 Hz bandwidth. In the horizontal direction the predicted displacement of the table peaks at the 8 Hz bandwidth. In both the Z- and X-directions the table displacement is above the NISTA criteria at one or two bandwidths. However, attenuation is seen in both directions at higher bandwidths.

In the second simulation it is seen that there is very little amplification of the floor vibrational energy at the table top for low frequency bandwidths. In the vertical direction, even with some amplification of noise in the frequency bands above 40 Hz the table is still under the NIST-A criterion. In

the horizontal direction amplification of the vibrational energy from the floor peaks at 60 Hz, but the table is still under the NIST-A criterion.

4 Embedded Pits Filled with Cohesionless Soil

4.1 Current Performance

4.1.1 Methodology

In order to measure ambient vibration levels present on the cap surfaces piezo based, low frequency accelerometers (VibraMetric model 1030 and PCB Piezotronics model 393B31) were placed in the vertical direction at various locations on the first two pits. For comparison ambient vibration measurements were taken on the floor inside the facility. Measurements were taken only in the vertical position for efficiency's sake and because previous studies of the neighboring Advanced Photon Source facility have shown that vibration levels in the horizontal direction are significantly lower, especially in the higher frequencies considered in this paper (Anton 2016). Therefore, if the vertical vibration levels can be said to comply with a certain criterion so can the horizontal vibration levels.

Acceleration data was taken by a Hewlett Packard (HP) E1432A 16 Channel 1.2 kSa/s Digitizer plus Digital Signal Processor with Data Physics Corporation's Signal Calc 620 Dynamic Signal Analyzer software. The acceleration data was converted into rms displacement and plotted using MatLab software. Showing vibration levels in terms of rms displacement has been used by these authors and others at the connected facility, the Advanced Photon Source (Anton 2016 and Royston 1996).

The results from pits 1 and 2 are evaluated against a set of vibration criteria. The two groups of criteria used are the generic vibration criteria (VC) and the NIST-A criterion. Developed for the semiconductor industry and metrology respectively both criteria are popular standards in a variety of technological fields. Both criteria use a standard proportional bandwidth (one-third octaves).

The generic vibration criteria consist of a number of curves (VC-A through VC-G). For VC-C through VC-G (i.e. the most relevant for this study) the curves are constant rms velocities from 1 Hz to 80 Hz. These velocities are shown as sloping curves of displacements for this paper. If the one-third octave band velocity spectrum lies below any curve it meets that criterion (Amick 2005).

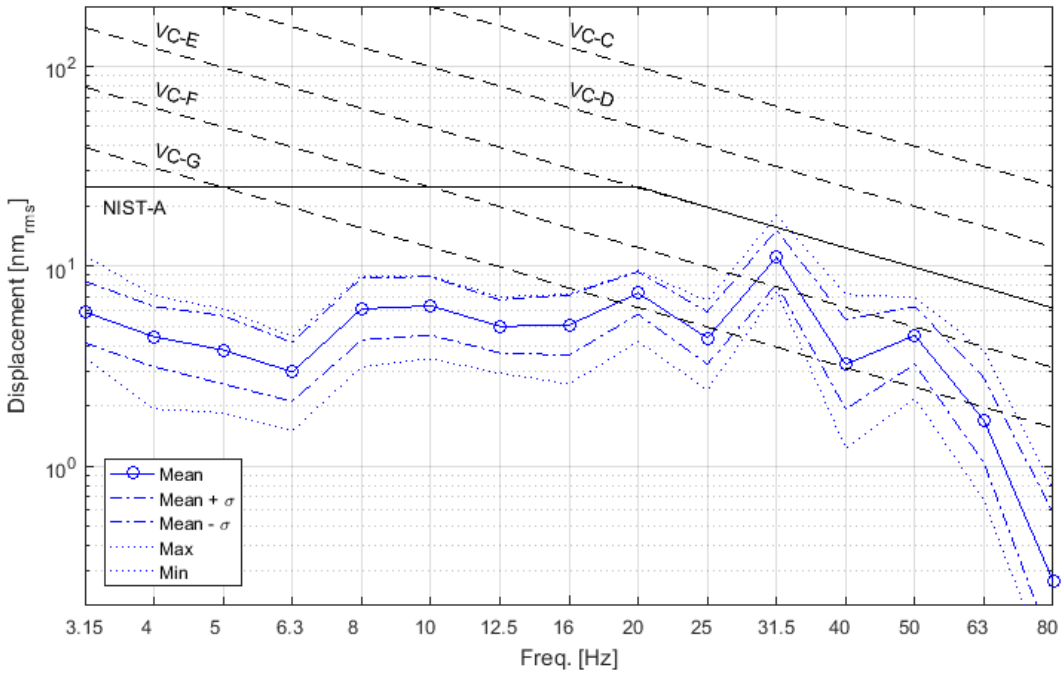

Figure 21: Pit 1 ambient vibration measurements and vibration criteria

The NIST-A criterion calls for vibration levels to be below a constant rms displacement of 25 nm from 1 Hz to 20 Hz and below a constant rms velocity of 3.1 µm/s from 20 Hz to 100 Hz.

To determine the effectiveness of the pits at reducing vibration levels the data collected on the pits is compared to the floor within the facility.

4.1.2 Results

For evaluation against the vibration criteria the ambient data is put into one-third octave bands (Figure 21 and Figure 22). For large areas, like the pit surfaces, it is suggested to display not only the mean of measurements taken but also the mean plus and minus one standard deviation, and the minimum and maximum value recorded for each band (Amick 2005).

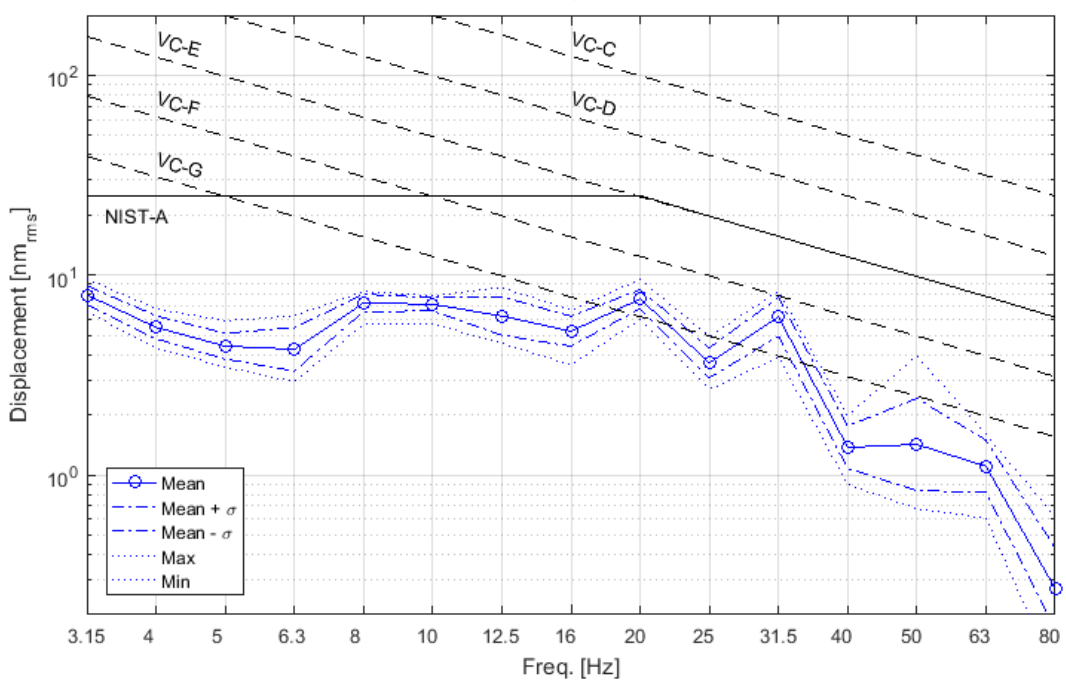

Figure 22: Pit 2 ambient vibration measurements and vibration criteria

To compare vibration measurement at different locations in one-third octave bands the mean values plus one standard deviation is used (Amick 2005).

4.1.3 Discussion

From figure 21 and figure 22 some general trends are seen in the vibration levels of both pits. On both Pit 1 and Pit 2 a consistent vibration level was measured in the low frequency bands (3.15 Hz through 20 Hz), with local minima at the 6.35 Hz frequency band. There is a relative spike seen on both pits at the 31.5 Hz band. This measured increase in vibrational energy is likely due to air handling equipment inside and around the building. Displacement values then diminish on both pits for bandwidths greater than 31.5 Hz.

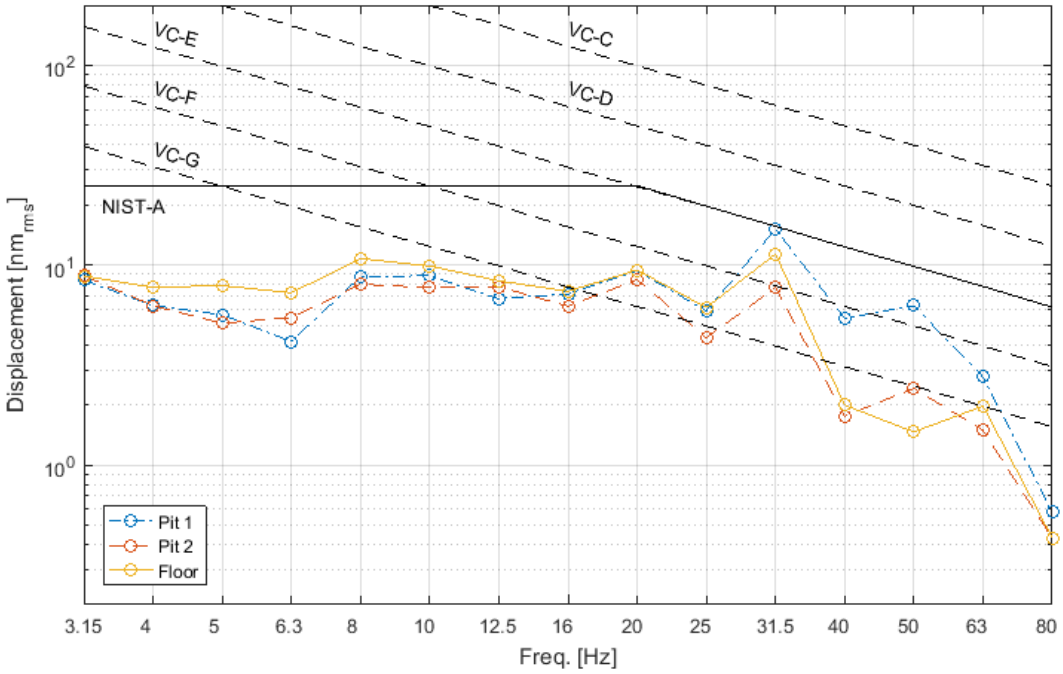

Figure 23: Pit 1, Pit2, and floor vibration measurements (mean plus standard deviation) and vibration criteria

Comparing Pit 1 to the vibration criteria in figure 21 it is seen that this pit meets the generic criterion VC-E. This criterion is suitable for the most demanding sensitive systems (Gordon 1999). Pit 1 also meets the NIST-A criterion, for the frequency range considered here. This criterion is a combination of the VC-E criterion with the requirement that rms displacement cannot be above 25 nm for frequency bands at or below 20 Hz (Amick 2005).

Pit 2 vibration levels and the vibration criteria are shown in figure 22. Pit 2, similarly to Pit 1, meets the NIST-A requirement. But, Pit 2 meets the stricter VC-F criterion.

Figure 23 shows the mean displacement plus one standard deviation for Pit 1, Pit 2 and the floor in the facility. Both pits have noticeably lower vibration levels than the floor in the 4 Hz through 10 Hz range. Above 20 Hz the pits diverge. It was found that Pit 1 has higher vibration levels than the

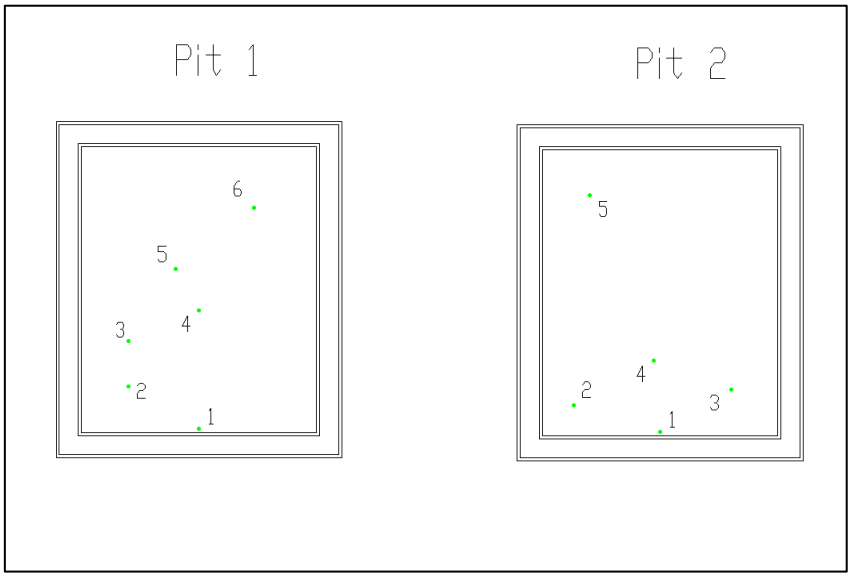

Figure 24: Accelerometer locations on Pit 1 and Pit 2 for impact tests

surrounding floor for bandwidths higher than 25 Hz. Pit 2 has lower vibration levels relative to the floor. Significantly, relatively lower vibration levels were seen on Pit 2 at the critical 31.5 Hz bandwidth. The single exception to relatively lower vibration levels at Pit 2 is at the 50 Hz bandwidth where higher vibration levels were measured on Pit 2 than the surrounding floor.

4.2 Finite Element Modeling of Filled Pits

4.2.1 Experimental Data

As with the sandbox structures, a realistic model of the filled pits needed to be built. To this end impact tests were made on Pit 1 and Pit 2. The impact force was provided by striking a sledge hammer sized impact hammer with a rubber tip (PCP 086D50) on the cap surface. Six on Pit 1 and five on Pit 2 piezo-based accelerometers were placed on the pit cap being tested (see Figure 24). For Pit 1 the impact hammer was struck near point 1 on each pit.

The data from the accelerometers and impact hammer were collected by a Hewlett Packard (HP) E1432A 16 Channel 1.2 kSa/s Digitizer plus Digital Signal Processor with Data Physics Corporation's

Signal Calc 620 Dynamic Signal Analyzer software. MatLab software was used to generate experimental force-response-functions for each accelerometer on the pit surfaces.

4.2.2 Finite Element Model

A 3-dimensional finite element model was created with Comsol Multiphysics software. This was done for both Pit 1 and Pit 2 -- excluding the surrounding floor, soil, and backfill material. The only difference between the two pits are the cap depth and fill material. The floor of each pit was set to a fixed boundary condition.

The "built in" options in the software were used for the concrete. As before the "build union" operation was used to unite all components of the models except for the fill material/side wall contact surfaces. For those surfaces a "thin elastic layer" was placed at the contact surfaces between the sand and the vertical walls of the pits. Like with the multi-footing FEM the horizontal stiffnesses of the “thin elastic layer” were set very high ($1x10^{20}$ N/m/m^2) to simulate a near bounded contact between the fill material and the pit walls. In the vertical direction the stiffness was set to 0. This was so tensile stresses were not created at the fill material/side wall contact surfaces.

The Young’s modulus, Poisson’s ratio, and density of the fill materials need to be inputted. Values of 0.33 and 1560 kg/m^3 were chosen for Poison's ratio and density, respectively. Void ratio was again chosen as 0.7. Equations 2 through 7 in Table were used to determine the shear modulus of the fill material for each pit. These equations yielded an average Young's modulus of sand of E=47 MPa with a standard deviation of σ = 18 MPa for Pit 1. For Pit 2 the average Young's modulus was E=74 MPa with at standard deviation of σ = 25 MPa. In Comsol the "Parametric Sweep" function was used to vary Young’s modulus from E-σ to E+σ for each pit. Values for eta were also varied using the “Parametric Sweep” function. The FEM data was compared with the experimental data and the Young’ modulus and damping that produced the lowest squared error were chosen.

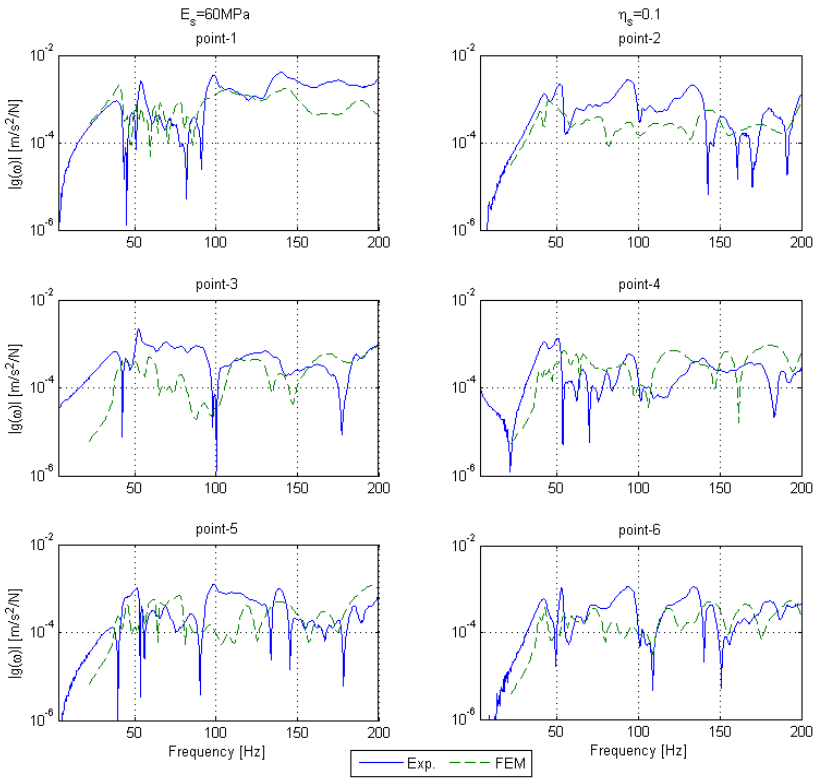

Figure 25: Pit 1 experimental and FE model force-response-functions for 6 sensor locations

A vertical force was with an amplitude of 1 N was applied to the location of the impact hammer strikes. Simulated force-response-functions were created in the same manner as the single-footing FEM.

4.2.3 Results

Figure 25 shows the experimental data and the FEM simulation for each sensor location on Pit 1 using the Young's modulus and damping that produced the lowest squared error. The Young's modulus was *E*=60 MPa and damping was eta=$10x10^{-2}$.

For Pit 2 values for Young's modulus and damping of 80 MPa and $8x10^{-2}$, respectively, produced the lowest squared error between the FEM and the experimental data. Figure 26 shows the experimental data and FEM simulation data at each sensor on Pit 2 using those parameters.

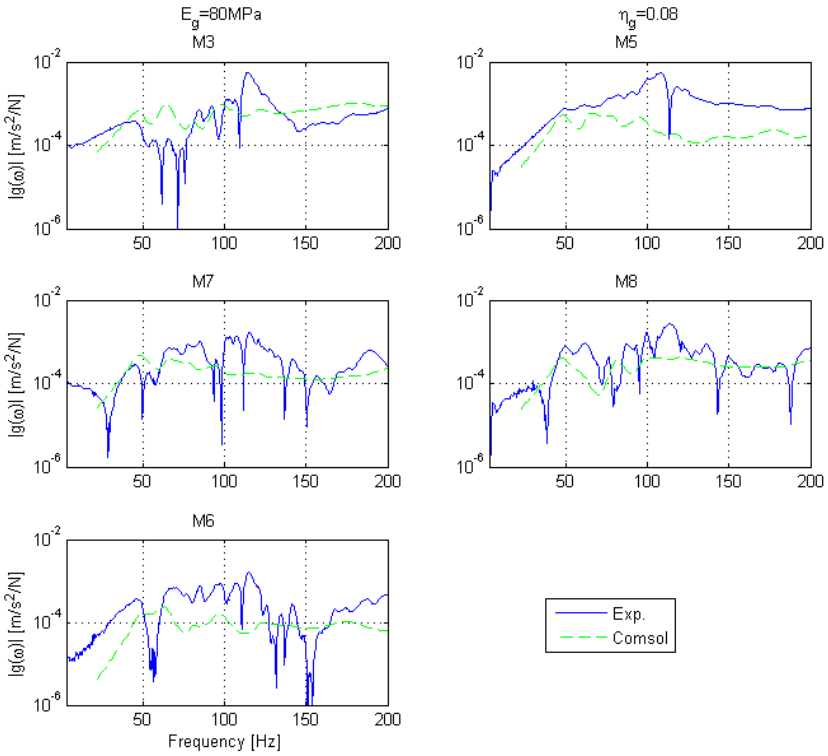

Figure 26: Pit 2 experimental and FE model force-response-functions for 5 sensor locations

For both pits the amount of damping, vibration levels, and some resonances are predicted by the FEM. Considering the complexity of the structures and vibration measurement errors this is good result from a simple FE model. Results below will show that this model be accurate for every point on the pits it is accurate enough to predict measurements like the ambient vibration measurements taken in section 4.1.

4.3 Design of future pits

4.3.1 Objectives

The vibrational energy levels for the floor surrounding the pits is shown in Figure 23. It can be seen that the highest rms displacement is at the 31.5 Hz 1/3 octave band. The objective of designing

filled pits is to minimize the amount of vibrational energy transferred to the pit cap at all bandwidths, but especially the 31.5 Hz bandwidth.

4.3.2 Parametric study

As with the CVD footing structures a parametric study was conducted. For the current pits the parameters were more limited than with the CVD structures. The area of the caps are already determined by the construction of the pits themselves. The fill material depth and mass of the caps are determined by the cap height.

A "Parametric Sweep" was performed in Comsol. The cap height and Young's modulus were varied. The cap height ranged from 0.1 m to 1.1 m and Young's Modulus was determined for each cap height by averaging the resulting moduli from the 5 equations in Table I.

Equation 13 was used to predict the damping of the fill material. The pressure and damping modeled at Pit 1 were used as p_1 and η_1. The pressure was calculated for the new cap height and used as p_2. The resulting η_2 was used as the loss factor for that simulation.

Prescribed displacement simultaneously in the X-, Y-, and Z-directions of the pit base was used to generate transfer functions. The mean displacement in all three directions on the cap surface was outputted from the FEM.

The vertical (Z-direction) surface displacement transfer functions were multiplied by the measured ambient floor vibration levels to create a predicted level of vibrations at the pit cap surface.

4.3.3 Results

Figure 27 shows resulting transfer functions from the “Parametric Sweep” of cap height. The horizontal directions (X and Y) had very similar results so for clarity only the X- and Z-directions are plotted. It can be seen that the cap height of 1.1 m has high resonant peaks in both the vertical and the horizontal directions. However, these peaks are located at higher frequency bands than most other

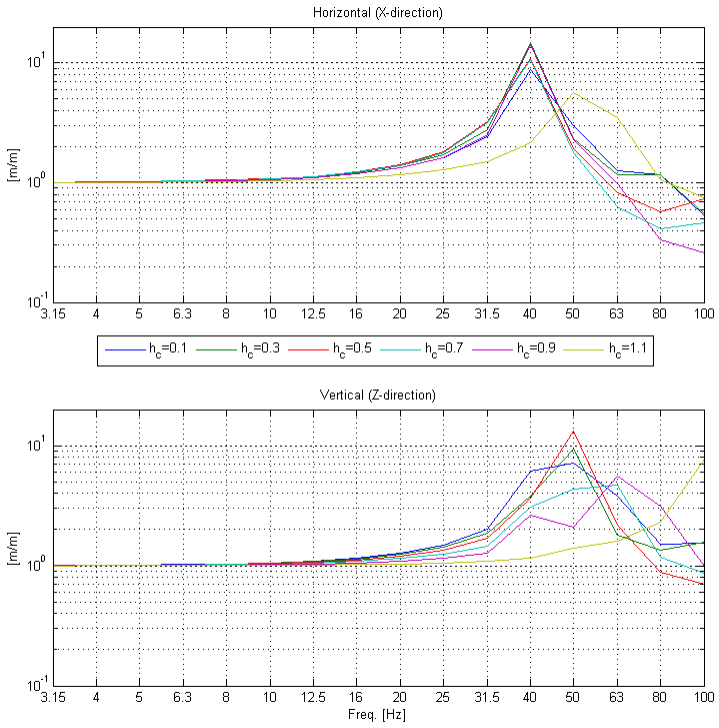

Figure 27: Transfer functions in the X- and Z-directions for multiple cap heights

simulated results. The calculated Young's modulus and damping for this cap height were 131 MPa and $6x10^{-2}$, respectively.

Figure 28 shows the predicted cap surface displacement, the measured floor displacement, and the NIST-A criterion in the vertical direction. The cap surface shows very little amplification of the vibrational energy present on the surrounding floor in low frequency bands. The amplification is noticeable above the 31.5 Hz frequency band and peaks the 80 Hz bandwidth. At those bandwidths the vibration levels at the cap surface are below the NIST-A criterion.

Data for the horizontal motion of the floor was not available. It is reasonable to expect the floor of the electron microscopy facility to be similar to the floor of the APS experiment hall. If that is the case the horizontal vibration levels should be below the NIST-A criterion.

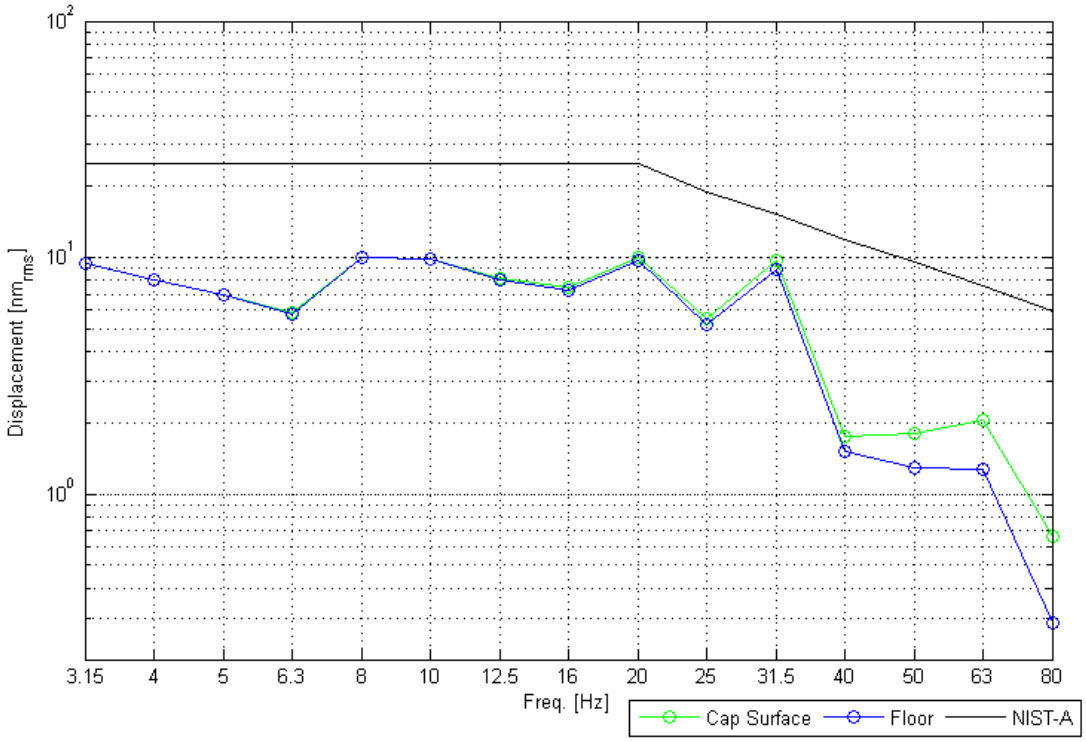

Figure 28: Average floor and cap surface displacement in 1/3 octave bands

5 Discussion

The combined vibration-damping structures and filled pits varied in many ways. First and foremost, the scale of each is quite different. Other differences are found in fill material used and the material supported by the sand or gravel.

The complexity of the pits was another difference between the two structures. This is mostly due to the fact that pit caps do not always move as a rigid body in the frequency range considered in this dissertation. The granite tables supported by the CVD structures are rigid well beyond the frequencies here. It was observed that there are no rigid body modes seen in the experimental data of Pit1. For Pit 2 some rigid body modes were observed in the 40 to 50 Hz range.

Despite all that the modeling of the structures and the design challenges for all were remarkably similar. Theories provided from the literature for moduli worked well for all structures studied. If Poisson's ratio was assumed to be 0.33 and a void ratio 0.7 the theories for moduli could be reasonably well applied to the CVD structure or the filled pits whether they are filled with sand or gravel.

5.1 Modeling of footing Structures and Filled Pits

When modeling the structures studied in this dissertation, whether it is an analytical or finite element model, some of the same factors affect the accuracy of those models.

Damping for cohesionless soils does not fit the Kelvin-Voigt model of a spring and dashpot in parallel. Instead, loss factor damping should be used to model damping as a constant over all frequencies. Damping should also be assumed to have an inverse relationship to pressure on the sand. This was not seen in this study but is supported in the literature (Iwasaki 1978).

When simulating dynamic behavior of these structures a few more factors must also be considered. First, the boundary conditions between the cohesionless soil and solids. Both "spring foundations" and "thin elastic layers" were used in Comsol to eliminate unreasonable tensile stresses at these boundaries. It was observed that the "spring foundation" is adequate for modeling the vertical

motion of these soils in structures it is inadequate at modeling any other modes of motion. The “thin elastic layer” should be used whenever more than vertical motion is of concern

Second, is mesh size. Strain was the highest for the cohesionless soil in the structures studied. Therefore, the element size on these components in the model are crucial. Through this study good modeling results were obtained by using a maximum element size of 0.0064 m and 0.0127 m at the top surface of the sand of the CVD structures and the pits, respectively.

Finally, shunting must be considered. If the sand is too stiff because of high bearing pressure or low sand depth, components in the model previously considered rigid can no longer assumed to be so. This was not an issue while modeling the filled pits. However, it did need to be accounted for in both of the CVD footing models. In those cases, it was bolts in the assembly that were taken into account to improve modeling results.

5.2 Design Challenges

As discussed in the parametric study sections, some parameters that lower the stiffness of the cohesionless soil also lower damping. Considering that most vibrational energy added from mechanical equipment is in the 10 to 60 Hz range. It makes it difficult to design structures with cohesionless soils that have low enough resonant frequencies to attenuate vibrational energy in the 10 to 60 Hz range while also having enough damping not to amplify lower frequency vibrations. Stiffer and more damped structures can be designed but then no attenuation of low frequency vibrations will occur.

There are other factors than the parameters studied here that are thought to affect stiffness and damping of cohesionless soils. Unfortunately, they are not as easy to assess. The tests needed for these to determine these parameters are outside the scope of this study.

For stiffness, void ratio is an important parameter. The listed numbers in the literature have a large range. To calculate void ratio, one needs a sample of the cohesionless soil before installation of the structures. This is not always an option when designing.

The literature suggests that damping is affected by the strain in the soil, how well graded the soil is, and the percent of fines and organic soils that are present. Throughout this study strain was assumed to be low in all soils. This is a safe assumption given the low levels of vibrational energy observe at these sights.

A well graded cohesionless soil has more particle size diversity than a poorly graded soil. Studies have found that more particle diversity a soil has the higher the damping of that soil. Relatedly a higher percentage of fines (particles passing through a #200 sieve) also increases damping of the soil (Wichtmann 2012). Both these properties can be determined by a sieve test. This is only practical if one has access to the soil during the design process.

For an accurate design of vibration isolation structures using cohesionless soil the soil should be obtained during the design process and tested. Vibration measurements should be taken on structures using the sampled soil at multiple pressures. Sieve tests and void ratio calculations could also be done. From there a structure that meet the needs of the uses of the structure, whether that is for electron microscopy or X-ray imaging.

6 Conclusions

6.1 Review of Purpose and Objectives of This Study

The purpose of this dissertation was to design structures that support sensitive equipment that require strict stability standards. For this, an understanding the dynamic behavior of cohesionless soils in vibration isolation structures was investigated.

The objectives in this work were as follows:

- Sand as part of CVD footing structure:
    - Objective 1: Generate force response functions from experimental footing model
    - Objective 2: Determine dynamic characteristics of sand using analytical models and experimental data
    - Objective 3: Design a finite element model that predicts the dynamic behavior of the footing structures
    - Objective 4: determine best configuration of sand in a CVD to isolate environmental noise at the APS
- Filled Pits:
    - Objective 1: Understand current performance of filled pits by a comparison of ambient vibration levels on the pits to the surrounding floor and standard vibration criteria
    - Objective 2: Design a finite element model of pits using impact data test data
    - Objective 3: Use parametric studies of the pits to determine the best design for isolating environmental noise at the CNM

All the listed objectives have been met and discussed in this dissertation. By completing all the objectives an understanding of soil mechanics in vibration isolation structures has been obtained. This

knowledge has led to an understanding of the parameters that are key in designing such structures, and from that, recommendations for the design of structures in the future.

6.2 Review of Contributions and Work

The objective of this dissertation study was to combine the knowledge of vibration isolation structures with the knowledge of the mechanics of cohesionless soil. What follows is a review of contributions this study has brought to that end.

6.2.1 Modeling Isolation Structures with Cohesionless Soil

Through the study of vibration measurements of experimental models and full-scale constructed structures an understanding of how to model vibration isolation structures that use cohesionless soil has been gained. For analytical models a spring with loss factor damping can be used to predict the behavior of the soil. By applying the analytical models to the experimental data stiffness and damping can be obtained. Further, the equation proposed by Gazetas for a rigid foundation over a layer of soil will yield the shear modulus of the soil. The experimental measurements also confirm the relationship between pressure on the soil and its modulus suggested in the literature.

Finite element models of all structures studied were constructed. Factors such as boundary conditions, mesh size, and shunting needed to be considered closely for the FEM to yield accurate results. The “thin elastic” boundary condition is recommended at the vertical sand/structure interfaces if more than just vertical motion is of concern. Mesh size on the sand surface must be sufficiently small to accurately model the relatively large displacements in the sand. If soil stiffness is high enough the dynamic behavior of other components, such as bolts, in the structures need to be considered and possibly modeled

For the CVD footing structures soil parameters discerned from the analytical models could be input into the FEM. This was not the case for the filled pits. A range of moduli and damping needed to

be calculated from the equations in the soil mechanics literature into the FEM to match the experimental data.

6.2.2 Designing Isolation structures with Cohesionless Soil

By building accurate models of existing structures the effect of parameters on the dynamic behavior of future structures can be understood. These parameters are footing radius, sand depth, number of footings, and mass of the supported structure. If all else remains the same, as footing radius increases the structures stiffness and damping increases. If sand depth increases stiffness will decrease. There is no effect on damping. As the number of footings increases so does stiffness and damping. Added mass will increase stiffness and decrease damping.

From these parameters two CVD structures and one filled pit were proposed to minimize the vibrational energy at the working surface of each structure.

6.3 Avenues of Future Work

This dissertation did accomplish all its objects set out above. However, there is still work to be done especially in the area of soil mechanics. The literature suggests a well graded soil with a relatively high percentage of fine grade should increase damping while decreasing the moduli of the material. However, this makes the proposed theories for or moduli in the literature less reliable. Iwasaki suggests testing of any natural sand that isn't uniform and has a relatively high amount of fine particles in it (1977). A better understanding of the role of particle size distribution has on the dynamic behavior of sand is need. Ideally this would lead to a design being able to predict the behavior of a cohesionless soil without conducting extensive testing on samples.

CITED LITERATURE

Advanced Photon Source. 2018. Advanced Photon Source: Welcome. Argonne National Laboratory n.d. [cited August 6, 2018]. Available from https://www.aps.anl.gov/About/Welcome.

Al-Homoud, Azm S., and Omar N. Al-Maaitah. "An experimental investigation of vertical vibration of model footings on sand." Soil Dynamics and Earthquake Engineering 15, no. 7 (1996): 431-445.

Amick, Hal, Steven G. Hardash, Paul E. Gillett, and Ronald J. Reaveley. "Design of stiff, low-vibration floor structures." In Vibration Control in Microelectronics, Optics, and Metrology, vol. 1619, pp. 180-192. International Society for Optics and Photonics, 1992.

Amick, Hal, and Michael Gendreau. "Construction vibrations and their impact on vibration-sensitive facilities." In Construction Congress VI: Building Together for a Better Tomorrow in an Increasingly Complex World, pp. 758-767. 2000.

Amick, Hal, Michael Gendreau, and Colin G. Gordon. "Facility vibration issues for nanotechnology research." In Proceedings of the Symposium on Nano Device Technology, Taiwan. 2002.

Amick, Hal, Michael Gendreau, Todd Busch, and Colin Gordon. "Evolving criteria for research facilities: vibration." In Buildings for Nanoscale Research and Beyond, vol. 5933, p. 593303. International Society for Optics and Photonics, 2005.

Anton, Jayson, Steven Kearney, and Deming Shu. "Ambient Vibration Measurement for APS floor at Sectors 29, 26, 23, and 21." (2016)

Argonne National Laboratory. 2018. Center for Nanoscale Materials: Quantum & Energy Materials. Argonne National Laboratory n.d. [cited August 6, 2016]. Available from: http://www.anl.gov/cnm/group/quantum-energy-materials.

Ashoori, Taha, and Keivan Pakiman. "Dynamic Response of Different Types of Shallow Foundation over Sandy Soils to Horizontal Harmonic Loading." International Journal of Geotechnical Earthquake Engineering (IJGEE) 6, no. 1 (2015): 1-14.

Baidya, D. K., G. Muralikrishna, and P. K. Pradhan. "Investigation of foundation vibrations resting on a layered soil system." Journal of geotechnical and geoenvironmental engineering 132, no. 1 (2006): 116-123.

Costa, Pedro Alves, Rui Calcada, and Antonio Silva Cardoso. "Influence of train dynamic modelling strategy on the prediction of track–ground vibrations induced by railway traffic." Proceedings of the Institution of Mechanical Engineers, Part F: Journal of Rail and Rapid Transit 226, no. 4 (2012): 434-450.

Das BM. Advanced soil mechanics. Crc Press; 2013.

Dobry, Ricardo, and George Gazetas. "Dynamic response of arbitrarily shaped foundations." Journal of geotechnical engineering 112, no. 2 (1986): 109-135.

Gazetas, George. "Analysis of machine foundation vibrations: state of the art." International Journal of Soil Dynamics and Earthquake Engineering 2, no. 1 (1983): 2-42.

Gazetas, George. "Formulas and charts for impedances of surface and embedded foundations." Journal of geotechnical engineering117, no. 9 (1991): 1363-1381.

Gazetas, George, and Kenneth H. Stokoe. "Free vibration of embedded foundations: theory versus experiment." Journal of geotechnical engineering 117, no. 9 (1991): 1382-1401.

Gordon, Colin G. "Generic criteria for vibration-sensitive equipment." In Vibration Control in Microelectronics, Optics, and Metrology, vol. 1619, pp. 71-86. International Society for Optics and Photonics, 1992.

Gordon, Colin G. "Generic vibration criteria for vibration-sensitive equipment." In Optomechanical Engineering and Vibration Control, vol. 3786, pp. 22-34. International Society for Optics and Photonics, 1999.

Hao, Hong, T. C. Ang, and Jay Shen. "Building vibration to traffic-induced ground motion." Building and Environment 36, no. 3 (2001): 321-336.

Hardin, Bobby O., and F. E. Richart Jr. "Elastic wave velocities in granular soils." Journal of Soil Mechanics & Foundations Div 89, no. Proc. Paper 3407 (1963).

Hardin, Bobby O. "Dynamic versus static shear modulus for dry sand." Materials research and standards 5, no. 5 (1965): 232-235.

Hardin, Bobby O. "The nature of damping in sands." Journal of the soil mechanics and foundations division 91, no. 1 (1965): 63-98.

Hardin, Bobby O., and William L. Black. "Sand stiffness under various triaxial stresses." Journal of Soil Mechanics & Foundations Div 92, no. ASCE# 4712 Proceeding (1966).

Ishibashi, Isao, and Xinjian Zhang. "Unified dynamic shear moduli and damping ratios of sand and clay." Soils and Foundations 33, no. 1 (1993): 182-191.

Iwasaki, Toshio, and Fumio Tatsuoka. "Effects of grain size and grading on dynamic shear moduli of sands." Soils and foundations 17, no. 3 (1977): 19-35.

Iwasaki, Toshio, Fumio Tatsuoka, and Yoshikazu Takagi. "Shear moduli of sands under cyclic torsional shear loading." Soils and Foundations 18, no. 1 (1978): 39-56.

Ju, Shen-Haw, and Hung-Ta Lin. "Analysis of train-induced vibrations and vibration reduction schemes above and below critical Rayleigh speeds by finite element method." Soil Dynamics and Earthquake Engineering 24, no. 12 (2004): 993-1002.

Ju, Shen Haw. "Finite element analysis of structure-borne vibration from high-speed train." Soil dynamics and earthquake engineering 27, no. 3 (2007): 259-273.

Kearney, Steven, and Deming Shu. A Survey of Floor Vibration Noise at All Sectors in the APS Experiment Hall. No. ANL/APS/LS-344. Argonne National Lab.(ANL), Argonne, IL (United States), 2016.

Kim, Y-S., K. Miura, S. Miura, and M. Nishimura. "Vibration characteristics of rigid body placed on sand ground." Soil Dynamics and Earthquake Engineering 21, no. 1 (2001): 19-37.

Kumar, Ankesh, Bappaditya Manna, and K. S. Rao. "Effect of Vertical Vibration on Block Foundation Resting on Homogeneous and Layered Medium." International Journal of Engineering Research 2, no. 7 (2013): 452-456.

Lak, Mohammad Amin, Geert Degrande, and Geert Lombaert. "The effect of road unevenness on the dynamic vehicle response and ground-borne vibrations due to road traffic." Soil Dynamics and Earthquake Engineering 31, no. 10 (2011): 1357-1377.

Macinante, Joseph A. Seismic mountings for vibration isolation. Wiley, 1984.

Mandal, A., D. K. Baidya, and D. Roy. "Dynamic response of the foundations resting on a two-layered soil underlain by a rigid layer." Geotechnical and Geological Engineering 30, no. 4 (2012): 775-786.

O'Keefe, Michael A., John H. Turner, John A. Musante, Crispin JD Hetherington, A. G. Cullis, Bridget Carragher, Ron Jenkins et al. "Laboratory design for high-performance electron microscopy." Microscopy Today 12, no. 3 (2004): 8-17.

Oztoprak, S., and M. D. Bolton. "Stiffness of sands through a laboratory test database." Géotechnique 63, no. 1 (2013): 54-70.

Pak, Ronald YS, and Bojan B. Guzina. "Dynamic characterization of vertically loaded foundations on granular soils." Journal of geotechnical engineering 121, no. 3 (1995): 274-286.

Royston, T. J. Vibration characteristics of an APS lab facility in building 401. No. LS-263 (ANL). Argonne National Lab., IL (United States), 1998.

Seed, H. Bolton, Robert T. Wong, I. M. Idriss, and Kohji Tokimatsu. "Moduli and damping factors for dynamic analyses of cohesionless soils." Journal of geotechnical engineering 112, no. 11 (1986): 1016-1032.

Soueid, Ahmad, Hal Amick, and Theodore Zsirai. "Addressing the environmental challenges of the NIST Advanced Measurement Laboratory." In Buildings for Nanoscale Research and Beyond, vol. 5933, p. 59330N. International Society for Optics and Photonics, 2005.

Streiffer, S., Vogt, S., Evans P.: Introduction: Early Science at the Upgraded APS. In: Early Science at the Upgraded Advanced Photon Source, pp. 1-18, https://www.aps.anl.gov/files/APS-Uploads/Aps-Upgrade/Beamlines/APS-U%20Early-Science-103015-FINAL.pdf

Tatsuoka, Fumio, Toshio Iwasaki, and Yoshikazu Takagi. "Hysteretic damping of sands under cyclic loading and its relation to shear modulus." Soils and Foundations 18, no. 2 (1978): 25-40.

Wichtmann, T., and Th Triantafyllidis. "Effect of uniformity coefficient on G/G max and damping ratio of uniform to well-graded quartz sands." Journal of geotechnical and geoenvironmental engineering 139, no. 1 (2012): 59-72.

Xu S, Lai B, Cai Z, Shu D. Vibration-damping structure for an x-ray microprobe supporting system. Review of scientific instruments. 2002; 73:1599-601.

APPENDICES

APPENDIX A: MATLAB Code for Single-Footing Model Results

A.1: Main Code

```
% Single Footing Exp, Anl, and FEM Results
close all; clear;
% cnt=1;
fgn=1;
%% Air spring effective stiffness and damping
% Plate setup parameters
mp=35.9; % [kg] Plate mass
% L=[.381 .4699 .0254]; % [m] Plate dimensions
% Frequency Offsets
fol=5;
foh=15;
% Load Exp. Data files
FNP='Data\SBP'; % Run Name
D=importdata(strcat(FNP,'_TF.txt'));
TF=D.data(:,2:13);
fp=D.data(:,1);
% Convert Data
S=[7.088 7.00 7.01 6.568 7.5 7.39]; % Sensitivities [V/g]
Sh=1e-3; %[V/N] Hammer Sensitivities
AmpI=[100*ones(1,3) 10*ones(1,3)]; % Accelerometer amplification
AmpH=10; % Hamper amplification
[m,n]=size(TF);
% Matrix allocation
T_e=zeros(m,n/2);
GA=zeros(m,n/2);
GV=zeros(m,n/2);
GDp=zeros(m,n/2);
% Real and Imaginary
for j=1:n/2
    T_e(:,j)=TF(:,(2*j-1))+1i*TF(:,(2*j)); %[g]/[N]
    GA(:,j)=9.81*T_e(:,j)*Sh*AmpH/(S(j)*AmpI(j)); %[m/s^2]/[N]
    GV(:,j)=GA(:,j)./(2*pi*fp);
    GDp(:,j)=GA(:,j)./(2*pi*fp).^2;
end
gp_ave=[mean(GDp(:,1:3),2) mean(GDp(:,4:6),2)];
gpm=abs(gp_ave);
phip=angle(gp_ave);
fT=fp(2)-fp(1);
I=round(fol/fT);
I_h=round(foh/fT);
[TFmax,Itf]=max(gp_ave(I:I_h,2));
fr=fp(I-1+Itf);
[~,I1]=min(abs(TFmax/2-gp_ave(I:(I+Itf),2)));
f1=fp(I+I1-1);
[~,I2]=min(abs(TFmax/2-gp_ave((I+Itf):I_h,2)));
f2=fp(Itf+I2+I-1);
Q=fr/(f2-f1);
zetab=1/(2*Q);
kbe=mp*(2*pi*fr)^2/(1-zetab^2)
cbe=2*zetab*sqrt(kbe*mp)
```

APPENDIX A (CONTINUED)

```
%% 2D Forced Vibration
% Exp. Data
RM='LMH';
FN='Data\';
S=[7.088 7.00 7.5 6.568 7.39 7.01 10.24 10.2 97.8e-3 20.84e-3]; %
Sensitivities [V/g] or [N/g]
Ampf1=[100; 100; 10; 10; 10; 10; 10; 10; 100; 10];
Ampf2=[100; 100; 10; 10; 10; 10; 10; 10; 10; 10];
Ampf=[Ampf2 Ampf2 Ampf1];
xl=[5 400];
ylm=[1e-9 2e-4];
% ylr=[1e-1 50];
ylp=[-3.5 3.5];
leg1=char('T1','T2','T3','T4','B1','B2','B3');
% leg2=char('Top mean','Bottom mean');
% ls=char('r-','g--','b:','m-.');
% ll=char('r','g','b','m','c','y','k');
% Matrix allocation
LIM=zeros(2,2,3,3);
GA=zeros(3201,7,3,3);
GAave=zeros(3201,2,3,3);
Gb=zeros(3201,3,3,3);
Gt=zeros(3201,4,3,3);
Gtave=zeros(3201,3,3);
Gbave=zeros(3201,3,3);
C=zeros(3201,7,3,3);
for TMN=1:3
    for SHN=1:3
        TM=RM(TMN);
        SM=RM(SHN);
        RN=strcat(TM,SM,'S'); % Run Name
        % Force Response Data
        TFt=importdata(strcat(FN,RN,'_TF_0916.txt'));
        TF=TFt.data(:,2:19);
        f=TFt.data(:,1);
        Ampft=Ampf(:,TMN);
        [m,n]=size(TF);
            ls=n/2+1;
        % Matrix allocation
        T_e=zeros(m,n/2);
        GAt=zeros(m,n/2);
        GV=zeros(m,n/2);
        GD=zeros(m,n/2);
        % Real and Imaginary
        for j=1:n/2
            T_e(:,j)=TF(:,(2*j-1))+1i*TF(:,(2*j)); %[g]/[N]
            GAt(:,j)=9.81*T_e(:,j)*S(ls)*Ampft(ls)/(S(j)*Ampft(j));
%[m/s^2]/[N]
            GV(:,j)=GAt(:,j)./(2*pi*f);
            GD(:,j)=GAt(:,j)./(2*pi*f).^2;
        end
        GA(:,:,TMN,SHN)=[GAt(:,6) -GAt(:,7:9) GAt(:,3:5)];

GAave(:,:,TMN,SHN)=[mean(GA(:,1:4,TMN,SHN),2),mean(GA(:,5:7,TMN,SHN),2)];
```

APPENDIX A (CONTINUED)

```
        Gb(:,:,TMN,SHN)=GD(:,3:5);
         Gt(:,:,TMN,SHN)=[GD(:,6) -GD(:,7:9)];
         Gtave(:,TMN,SHN)=mean(Gt(:,:,TMN,SHN),2);
         Gbave(:,TMN,SHN)=mean(Gb(:,:,TMN,SHN),2);
         % Coherence Data
         Ctt=importdata(strcat(FN,RN,'_C_0916.txt'));
         Ct=[Ctt.data(:,6:9) Ctt.data(:,3:5)];
         C(:,:,TMN,SHN)=Ct;
    end
end
get=abs(Gtave);
geb=abs(Gbave);
phiet=angle(Gtave);
phieb=angle(Gbave);
lf=length(f);
FT=f(2)-f(1);
LIMI=round(LIM/FT);
omega=2*pi*f;
%% 2D Model: g2=[x1/f; x2/f]
% Optimizing ks and cs
% Model Setup
rp=4.25*.0254; % contact plate radius [m]
Ap=pi*rp^2; % contact area [m]^2
hs=[26.2 61.9 146]*1e-3; % [m] sand height
kest=60e6*Ap./hs;
% properties considered
st=.07;
range=(1+st):st:2;
spread=[flip(1./range) 1 range];
ks=1.5*kest(3)*spread;
st2=.2;
range2=(1+st2):st:2;
spread2=[flip(1./range2) 1 range2];
etas=1e-5*spread2;
% cs=ks'*etas;
lks=length(ks);
lcs=length(etas);
s=1;%lks*lcs
%% Results after optimizing
Kse=1e7*[6.859  4.0809 2.8202;
    8.013 6.1213 3.8258;
    10.09 7.7618 5.12]; % Sand stiffness optimized from 2D Model
etase=[.0205 .0679 .0294;
    .0112 .1040 .0357;
    .0295 .0596 .0562];% Sand damping optimized from 2D Model
etasf=mean(mean(etase))
%% optimize ks and cs with 2D Analytical model
% Sand Parameters
mt=[33.43 31.07 31.07; 58.62 56.26 56.26; 84.19 81.69 81.69]; % [kg] mass
above sand
ms=[1.681 3.963 9.352]; % [kg]  sand mass
rhos=ms./(Ap*hs);
% Air Bearing Parameters
mb=38.04; % [kg] Plate mass and cylinder
```

APPENDIX A (CONTINUED)

```
% allocate matrices
m1=zeros(3,3);
GDmt=zeros(lf,2,s);
b2=zeros(s,2);
RDm=zeros(lf,s);
SQE=zeros(1,s);
K=zeros(3,3);
C=zeros(3,3);
GDm=zeros(lf,2,3,3);
gmt=zeros(lf,3,3);
gmb=zeros(lf,3,3);
phim=zeros(lf,2,3,3);
RDmm=zeros(lf,3,3);
phirm=zeros(lf,3,3);
GAmt=zeros(lf,2,s);
% Set offsets for error calculations
fT=f(2)-f(1);
fol=5;
foh=[350 300 250; 300 250 225; 250 200 150];
Il=round(fol/fT);
Ih=round(foh/fT);
cnt=1;
for TMN=1:3
    for SHN=1:3
        TM=RM(TMN);
        SM=RM(SHN);
        RN=strcat(TM,SM,'S'); % Run Name
        m2=mb+1/2*ms(SHN); % [kg] bottom mass
        m1(TMN,SHN)=mt(TMN,SHN)+1/2*ms(SHN);% [kg] Top mass
        ct=0;
        M2=[m1(TMN,SHN) 0; 0 m2];
%         for i=1:lks
%             for j=1:lcs
                ct=ct+1;
                [TMN SHN ct];
                kst=Kse(TMN,SHN);
                etast=etase(TMN,SHN);
                kbt=kbe;%kbe(TMN,SHN);
                cbt=cbe;%cbe(TMN,SHN);
                K2=[kst*(1+1i*etast) -kst*(1+1i*etast);
                    -kst*(1+1i*etast) kst*(1+1i*etast)+kbt];%[Kse(TMN,SHN) -
Kse(TMN,SHN); -Kse(TMN,SHN) Kse(TMN,SHN)+kb2];%[ks(i) -ks(i); -ks(i)
ks(i)+kb2];
                C2=[0 0;
                    0 cbt];%

                for u=1:lf
                    A=-M2*omega(u)^2+1j*C2+K2; %[N]/[m] *omega(u)
                    GDmt(u,:,ct)=transpose(-A\[1; 0]); %[m]/[N]
                end
%                 b(ct,:)=[ks(i) etas(j)];
                GAmt(:,:,ct)=GDmt(:,:,ct).*[omega omega].^2;
                ER=GAmt(Il:Ih(TMN,SHN),:,ct)-
GAave(Il:Ih(TMN,SHN),:,TMN,SHN);% Error Vector
```

APPENDIX A (CONTINUED)

```
                SQEt=ER'*ER; % Squared error error vector (ER) x complex
congigate of ER
                SQE(ct)=sum(diag(SQEt)); % 2x~many~ X ~many~x2 = 2x2 Diagonal
is Top-Top and Bottom-Bottom
%             end
%         end
        % Minimum squared error
        [emin,Ier]=min(SQE);
        K(TMN,SHN)=b2(Ier,1);
        C(TMN,SHN)=b2(Ier,2);
        GDm(:,:,TMN,SHN)=GDmt(:,:,Ier);
        gmt(:,TMN,SHN)=abs(GDmt(:,1,Ier));
        gmb(:,TMN,SHN)=abs(GDmt(:,2,Ier));
        phim(:,:,TMN,SHN)=angle(GDmt(:,:,Ier));
        GAm(:,:,TMN,SHN)=GAmt(:,:,Ier);
        gamt(:,TMN,SHN)=abs(GAmt(:,1,Ier));
        gamb(:,TMN,SHN)=abs(GAmt(:,2,Ier));
        figure(fgn)
        subplot(3,3,cnt);%subplot(3,3,cnt)
        semilogy(f,get(:,TMN,SHN),f,geb(:,TMN,SHN))
        hold on
        semilogy(f,gamt(:,TMN,SHN)./(2*pi*f).^2,'r--
',f,gamb(:,TMN,SHN)./(2*pi*f).^2,'g--');
        hold off
        title({['Sand Height:' num2str(round(hs(SHN)*1e3)) 'mm'] ['Top Mass:'
num2str(round(mt(TMN,SHN))) 'kg']})
        if cnt==7
            legend('Exp. Top Plate','Exp. Bottom Plate','Model Top
Plate','Model Bottom
Plate','Location','southoutside','Orientation','horizontal')%legend('Exp.','M
odel','FEM','Location','northeast')
        end
        xlim(xl);
        ylim(ylm);
        if cnt>2%6
            xlabel('Frequency Hz')
        end
%         if cnt==1 || cnt==4 || cnt==7
%             ylabel('|g(\omega)| [m/N)')
%         end
        ylabel('|g(\omega)| [m/N)')
        grid on
        cnt=cnt+1;
    end
end
fgn=fgn+1;
%% determining Moduli for single foot SB
mtot=mt+[ms; ms; ms]/2;
rc=4.5*.0254; % anular cylinder inner radius [m]
Ac=pi*rc^2; % cylinder area [m]^2
H=[hs;hs;hs];
e=.75; % Void Ratio of sand
nus=.33;%.2:.05:.4; % Poisson's ratio of sand
ct=1;
```

APPENDIX A (CONTINUED)

```
Pze=mtot*9.81/Ap;
S=9;%length(nus);
Esm=zeros(3,3,S);
Ese=zeros(3,3,S);
SQE=zeros(1,S);
P=zeros(S,3);
mm=mean(mtot,2);

for i=1:9
    for j=1:3
        for k=1:3
        Esm(j,:,ct)=Esf(rp,mtot(j,k),e,nus,1,i); % MPa
        end
    end
        Gse=Kse*(1-nus)./(4*rp*(1+1.28*rp./H)); % Gazetas 1983
        Ese(:,:,ct)=2*Gse*(1+nus)/1e6;
        ER=Ese(:,:,ct)-Esm(:,:,ct);
        SQE(ct)=sum(sum(ER.*ER));
        ct=ct+1;
end
[~,Ie]=min(SQE);
% nusf=nus(Ie);
Eseo=Ese(:,:,Ie);% MPa
Esmo=Esm(:,:,Ie);% MPa
ls=char('r-','g--','b:','m-.');
ll=char('r','g','b','m','c','y','k');
leg2=char('Pak 95','Hardin 63','Hardin 63','Seed 86','Iwasaki 78','Iwasaki
78','Oztoprak 13','Oztoprak 13','Al-Homoud 96');
figure(fgn)
for i=1:3
    plot(Pze(:,i)/1e3,Eseo(:,i),strcat(ll(i),'o'))
    hold on
   if i==1
       lgt=strcat('Sand Height:',num2str(round(hs(i)*1e3)),'mm');
   else
       lgt=char(lgt,strcat('Sand Height:',num2str(round(hs(i)*1e3)),'mm'));
   end
end
plot(Pze(:,1)/1e3,mean(Esmo,2),'bs--')
hold off
grid on
legend(char(lgt,leg2(Ie,:)),'Location','Northwest')
xlabel('Bearing Pressure [kPa]')
ylabel('Youngs Modulus of Sand [MPa]')
fgn=fgn+1;
Esmf=mean(Esmo,2)
Gsmf=Esmf/(2*(1+nus));
% Matrix allocation
kfm=zeros(3,3);
for TMN=1:3
    for SHN=1:3
        kfm(TMN,SHN)=Gsmf(TMN)*(4*rp*(1+1.28*rp./hs(SHN)))/(1-nus);
    end
end
```

APPENDIX A (CONTINUED)

```
%%
Gfm=zeros(2,lf,3,3);
% Model Final Model using mean Gs
for TMN=1:3
    for SHN=1:3
        C2f=[0 0;
            0 cbe];
        M2f=[m1(TMN,SHN) 0;
            0 m2];
        K2f=[kfm(TMN,SHN)*(1+1i*etasf) -kfm(TMN,SHN)*(1+1i*etasf);
            -kfm(TMN,SHN)*(1+1i*etasf) kfm(TMN,SHN)*(1+1i*etasf)+kbe];
        for u=1:lf
            A=-M2f*omega(u)^2+1j*C2f*omega(u)+K2f; %[N]/[m]
            Gfm(:,u,TMN,SHN)=A\[1; 0]; %[m]/[N]
        end
    end
end
gfm=abs(Gfm);
%% Comsol Data
% Import data
Gt=ImpCom2(strcat('ComData\ComData2.txt'),6,inf);
pn=9; % Parameter Number [Number of parameter combonations used in Comsol] 3
X 3 X 2 = 18 (3 sand heights, 3 top masses, 1 force locations)
lg=length(Gt);
ld=lg/pn;
hst=[.026 .062 .146];
hb=[.05 .1 .15];
num=[1 2 3]';
% Matrix allocation
GC=zeros(ld,2,3,3);
Esm=zeros(3,3);
% g6D=zeros(ld,2,3,3);
fc=Gt(1:ld,4);
for i=1:pn
    shm=Gt(ld*(i-1)+1,1)==hst;
    SHN=shm*num;
    tmm=Gt(ld*(i-1)+1,2)==hb;
    TMN=tmm*num;
    Esm(TMN,SHN)=Gt(ld*(i-1)+1);
%     if G(ld*(i-1)+1,3)==1;
      GC(:,:,TMN,SHN)=Gt((ld*(i-1)+1):ld*i,5:6);
%     else
%         g6D(:,:,TMN,SHN)=G((ld*(i-1)+1):ld*i,6:7);
%     end
end
gct=permute(GC(:,1,:,:),[1 3 4 2]);
gcb=permute(GC(:,2,:,:),[1 3 4 2]);
%% Plot results
% All 2DoF Data
xl=[0 350];
yld=[1e-10 2e-4];
cnt=1;
% Top Plate Motion
for TMN=1:3
```

APPENDIX A (CONTINUED)

```
    for SHN=1:3
        figure(fgn)
        subplot(3,3,cnt);
        semilogy(f,get(:,TMN,SHN))%
        hold on
        semilogy(f,gfm(1,:,TMN,SHN),'r--')%
        semilogy(fc,gct(:,TMN,SHN),'g--')%
        hold off
        title({['Sand Height:' num2str(round(hs(SHN)*1e3)) 'mm'] ['Top Mass:'
num2str(round(mt(TMN,SHN))) 'kg']})
        if cnt==8

legend('Exp.','Model','FEM','Location','southoutside','Orientation','Horizont
al')
        end
        xlim(xl);
        ylim(yld);
        if cnt>2%6
            xlabel('Frequency Hz')
        end
        ylabel('|g(\omega)| [m/N)')
        grid on
        cnt=cnt+1;
    end
end
fgn=fgn+1;
%% FEM Threaded Rods
for TMN=1:3
    TM=RM(TMN);
    SM=RM(1);
    RN=strcat(TM,SM,'S'); % Run Name
    FNt=strcat('Data\ComData',RN,'kr.txt');
    GCt=ImpComkr(FNt,9,inf);
    fcr=GCt(:,1);
    gcrt(:,TMN)=GCt(:,2);
    gcrb(:,TMN)=GCt(:,3);
end
%% Plot results Threaded Rod results
xl=[0 350];
ylr=[1e-1 2e2];
yld=[1e-10 2e-4];
cnt=1;
% Top Plate Motion
for TMN=1:3
    for SHN=1
        figure(fgn)
        subplot(3,1,cnt);%subplot(3,3,cnt)
        semilogy(f,get(:,TMN,SHN))%,f,geb(:,TMN,SHN))
        hold on
        semilogy(fcr,gcrt(:,TMN,SHN),'g--')%,fc,GC(:,2,TMN,SHN),'g:')
        hold off
        title({['Sand Height:' num2str(round(hs(SHN)*1e3)) 'mm'] ['Top Mass:'
num2str(round(mt(TMN,SHN))) 'kg']})
        if cnt==3
```

APPENDIX A (CONTINUED)

```
legend('Exp.','FEM','Location','southoutside','Orientation','Horizontal')
        end
        xlim(xl);
        ylim(yld);
        if cnt>2
            xlabel('Frequency Hz')
        end
        ylabel('|g(\omega)| [m/N)')
        grid on
        cnt=cnt+1;
    end
end
fgn=fgn+1;
%%
```

A.2: Code to calculate Young's modulus from theoretical equations

```
% equations for shear modulus
function Es=Esf(Ro,mt,e,nu,nf,eqn)
    % Sand Properties
    Af=nf*pi*Ro.^2; %[m^2]
    Pakg=98066.5; % Pacals per kgf/cm^2
    Papsf=47.88; % Pascals per lbf/ft^2
    pa=100e3; % Atmospheric pressure
    % Pressure from Plate and sand
    Pr=mt*9.81./(Af); % static bearing pressure
    Pm=Pr*nu/(1-nu);
    p=(Pr+2*Pm)/3;
    % Shear Mod. Pak and Guzina
    Go1=1.64e6*(2.17-e).^2./(1+e); %Pa
    Gs1=Go1.*(Ro).^.1.*(Pr/1e3).^.5; % Pa
    E1=Gs1*2*(nu+1)/1e6; % MPa
    % shear mod Iwasaki Tatsuoka Round Ottawa sands
    G2kg=700*(2.17-e)^2/(1+e)*sqrt(p/Pakg);
    Gs2=G2kg*Pakg;
    E2=2*Gs2*(nu+1)/1e6;
    % shear mod Iwasakit Tatsuoka Angular Ottawa sands
    G3kg=362*(2.97-e)^2/(1+e)*sqrt(p/Pakg);
    Gs3=G3kg*Pakg;
    E3=2*Gs3*(nu+1)/1e6;
    % shear mod Seed 1986
    K2=52.5; % Ranges from 30 to 75
    G4psf=1e3*K2*sqrt(Pm/Papsf);
    Gs4=G4psf*Papsf;
    E4=2*Gs4*(nu+1)/1e6;
    % shear mod Iwasaki 1978 Low Strain: gamma=1e-6
    G5kg=900*(2.17-e)^2/(1+e)*(p/Pakg).^.4;
    Gs5=G5kg*Pakg;
    E5=2*Gs5*(nu+1)/1e6;
    % shear mod Iwasaki 1978 High Strain: gamma=1e-4
    G6kg=700*(2.17-e)^2/(1+e)*(p/Pakg).^.5;
    Gs6=G6kg*Pakg;
    E6=2*Gs6*(nu+1)/1e6;
    % shear mod Oztoprak 2013 Low Strain: gamma=1e-5
```

APPENDIX A (CONTINUED)

```
    A7=5760;
    m7=.49;
    Gs7=A7*pa/(1+e)^3*(p/pa).^m7;
    E7=2*Gs7*(nu+1)/1e6;
    % shear mod Oztoprak 2013 Higher Strain: gamma=1e-4
    A8=5520;
    m8=.51;
    Gs8=A8*pa/(1+e)^3*(p/pa).^m8;
    E8=2*Gs8*(nu+1)/1e6;
    % shear mod Al-Homoud 1996
    Go9=G5kg;
    G9kg=Go9.*(Ro).^.1.*(Pr/1e3).^.5;
    Gs9=G9kg*Pakg;
    E9=2*Gs9*(nu+1)/1e6;
    EM=[E1 E2 E3 E4 E5 E6 E7 E8 E9];
    Es=EM(eqn);
```

A.3: Code that imports FEM Data

```
function ComData2 = ImpCom2(filename, startRow, endRow)
%IMPORTFILE1 Import numeric data from a text file as a matrix.
%   COMDATA2 = IMPORTFILE1(FILENAME) Reads data from text file FILENAME for
%   the default selection.
%
%   COMDATA2 = IMPORTFILE1(FILENAME, STARTROW, ENDROW) Reads data from rows
%   STARTROW through ENDROW of text file FILENAME.
%
% Example:
%   ComData2 = importfile1('ComData2.txt', 1, 635);
%
%    See also TEXTSCAN.

% Auto-generated by MATLAB on 2018/07/24 09:48:16

%% Initialize variables.
if nargin<=2
    startRow = 1;
    endRow = inf;
end

%% Read columns of data as strings:
% For more information, see the TEXTSCAN documentation.
formatSpec = '%15s%27s%25s%21s%35s%s%[^\n\r]';

%% Open the text file.
fileID = fopen(filename,'r');

%% Read columns of data according to format string.
% This call is based on the structure of the file used to generate this
% code. If an error occurs for a different file, try regenerating the code
% from the Import Tool.
dataArray = textscan(fileID, formatSpec, endRow(1)-startRow(1)+1,
'Delimiter', '', 'WhiteSpace', '', 'HeaderLines', startRow(1)-1,
'ReturnOnError', false);
```

APPENDIX A (CONTINUED)

```
for block=2:length(startRow)
    frewind(fileID);
    dataArrayBlock = textscan(fileID, formatSpec, endRow(block)-
startRow(block)+1, 'Delimiter', '', 'WhiteSpace', '', 'HeaderLines',
startRow(block)-1, 'ReturnOnError', false);
    for col=1:length(dataArray)
        dataArray{col} = [dataArray{col};dataArrayBlock{col}];
    end
end

%% Close the text file.
fclose(fileID);

%% Convert the contents of columns containing numeric strings to numbers.
% Replace non-numeric strings with NaN.
raw = repmat({''},length(dataArray{1}),length(dataArray)-1);
for col=1:length(dataArray)-1
    raw(1:length(dataArray{col}),col) = dataArray{col};
end
numericData = NaN(size(dataArray{1},1),size(dataArray,2));

for col=[1,2,3,4,5,6]
    % Converts strings in the input cell array to numbers. Replaced non-
numeric
    % strings with NaN.
    rawData = dataArray{col};
    for row=1:size(rawData, 1);
        % Create a regular expression to detect and remove non-numeric
prefixes and
        % suffixes.
        regexstr = '(?<prefix>.*?)(?<numbers>([-
]*(\d+[\,]*)+[\.]{0,1}\d*[eEdD]{0,1}[-+]*\d*[i]{0,1})|([-
]*(\d+[\,]*)*[\.]{1,1}\d+[eEdD]{0,1}[-+]*\d*[i]{0,1}))(?<suffix>.*)';
        try
            result = regexp(rawData{row}, regexstr, 'names');
            numbers = result.numbers;

            % Detected commas in non-thousand locations.
            invalidThousandsSeparator = false;
            if any(numbers==',');
                thousandsRegExp = '^\d+?(\,\d{3})*\.{0,1}\d*$';
                if isempty(regexp(thousandsRegExp, ',', 'once'));
                    numbers = NaN;
                    invalidThousandsSeparator = true;
                end
            end
            % Convert numeric strings to numbers.
            if ~invalidThousandsSeparator;
                numbers = textscan(strrep(numbers, ',', ''), '%f');
                numericData(row, col) = numbers{1};
                raw{row, col} = numbers{1};
            end
        catch me
        end
```

APPENDIX A (CONTINUED)

```
    end
end


%% Replace non-numeric cells with NaN
R = cellfun(@(x) ~isnumeric(x) && ~islogical(x),raw); % Find non-numeric
cells
raw(R) = {NaN}; % Replace non-numeric cells

%% Create output variable
ComData2 = cell2mat(raw);
```

APPENDIX B: MATLABE Code for Parametric Study of CVD Structures

B.1: Main Code

```
%% Parametric Study of Sandbox Footings
% equations for shear modulus From Table I page 10 of Thesis
% Gazetas 1983 for stiffness
clear all;
Mp=1000:100:10000;%3*1.5*.75*2750;%
Ro=(1:.25:12)*.0254;%4*.0254;.04;%
hs=(1:.25:20)*.0254;%.4;%.4%.4;%.5;%
n=4:16; % Number of feet%4;%3;%
for i=1:4
    if i==1
        Mpt=Mp; % Plate Mass [kg]
        Rot=mean(Ro); % Footing Radius [m]
        hst=mean(hs); % Sand depth [m]
        nt=4;
    elseif i==2
        Mpt=mean(Mp); % Plate Mass [kg]
        Rot=Ro; % Footing Radius [m]
        hst=mean(hs); % Sand depth [m]
        nt=4;
    elseif i==3
        Mpt=mean(Mp); % Plate Mass [kg]
        Rot=mean(Ro); % Footing Radius [m]
        hst=hs; % Sand depth [m]
        nt=4;
    else
        Mpt=mean(Mp); % Plate Mass [kg]
        Rot=mean(Ro); % Footing Radius [m]
        hst=mean(hs); % Sand depth [m]
        nt=n;
    end
    % Sand Properties
    Aft=nt*(pi*Rot.^2); %[m^2]
    e=.7;%mean(.3:.15:.75); % Sand void ratio
    rhos=1500; % Sand density [kg/m^3]
    nus=.33;
    Pakg=98066.5; % Pacals per kgf/cm^2
    Papsf=47.88; % Pascals per lbf/ft^2
    pa=100e3; % Atmospheric pressure
    % Pressure from Plate and sand
    Pr=Mpt*9.81./(Aft); % static bearing pressure (four feet)
    Pm=Pr*nus/(1-nus);
    p=(Pr+2*Pm)/3;
    % Shear Mod. Pak and Guzina
    Go1=1.64e6*(2.97-e).^2./(1+e); %Pa
    Gs1=Go1.*(Rot).^.1.*(Pr/1e3).^.5; % Pa
    E1=Gs1*2*(nus+1)/1e6; % MPa
    % shear mod Hardin Round Ottawa sands
    G2kg=700*(2.17-e)^2/(1+e)*sqrt(p/Pakg);
    Gs2=G2kg*Pakg;
    E2=2*Gs2*(nus+1)/1e6;
    % shear mod Hardin Angular Ottawa sands
    G3kg=362*(2.97-e)^2/(1+e)*sqrt(p/Pakg);
```

APPENDIX B (CONTINUED)

```
Gs3=G3kg*Pakg;
  E3=2*Gs3*(nus+1)/1e6;
% shear mod Seed 1986
K2=52.5; % Ranges from 30 to 75
G4psf=1e3*K2*sqrt(Pm/Papsf);
Gs4=G4psf*Papsf;
E4=2*Gs4*(nus+1)/1e6;
% shear mod Iwasaki 1978 Low Strain: gamma=1e-6
G5kg=900*(2.17-e)^2/(1+e)*(p/Pakg).^.4;
Gs5=G5kg*Pakg;
E5=2*Gs5*(nus+1)/1e6;
% shear mod Oztoprak 2013 Low Strain: gamma=1e-5
A6=5760;
m6=.49;
Gs6=A6*pa/(1+e)^3*(p/pa).^m6;
E6=2*Gs6*(nus+1)/1e6;
% Stiffness
kseq1=nt.*4.*Gs1.*Rot.*(1+1.28*Rot./hst)/(1-nus);
kseq2=nt.*4.*Gs2.*Rot.*(1+1.28*Rot./hst)/(1-nus);
kseq3=nt.*4.*Gs3.*Rot.*(1+1.28*Rot./hst)/(1-nus);
kseq4=nt.*4.*Gs4.*Rot.*(1+1.28*Rot./hst)/(1-nus);
kseq5=nt.*4.*Gs5.*Rot.*(1+1.28*Rot./hst)/(1-nus);
kseq6=nt.*4.*Gs6.*Rot.*(1+1.28*Rot./hst)/(1-nus);
if i==1
    wnm1=[sqrt(kseq1./Mpt);
        sqrt(kseq2./Mpt);
        sqrt(kseq3./Mpt);
        sqrt(kseq4./Mpt);
        sqrt(kseq5./Mpt);
        sqrt(kseq6./Mpt)];
    etar1=sqrt(mean(p)./p);
elseif i==2
    wnr1=[sqrt(kseq1./Mpt);
        sqrt(kseq2./Mpt);
        sqrt(kseq3./Mpt);
        sqrt(kseq4./Mpt);
        sqrt(kseq5./Mpt);
        sqrt(kseq6./Mpt)];
    etar2=sqrt(mean(p)./p);
elseif i==3
    wnh1=[sqrt(kseq1./Mpt);
        sqrt(kseq2./Mpt);
        sqrt(kseq3./Mpt);
        sqrt(kseq4./Mpt);
        sqrt(kseq5./Mpt);
        sqrt(kseq6./Mpt)];
else
    wnn1=[sqrt(kseq1./Mpt);
        sqrt(kseq2./Mpt);
        sqrt(kseq3./Mpt);
        sqrt(kseq4./Mpt);
        sqrt(kseq5./Mpt);
        sqrt(kseq6./Mpt)];
    etar3=sqrt(mean(p)./p);
```

APPENDIX B (CONTINUED)

```
    end
end
yl=[0 1000];
ls=char('r-','b-','b--','m--','k:','c--');
fn=wnn1/(2*pi);
%% Plot Young's Moduli
fgn=1;
figure(fgn)
for i=1:6
    subplot(2,2,1)
    plot(Mp,wnm1(i,:),ls(i,:))
    xlim([1500 10000])
    xlabel('Table Mass [kg]')
    ylim(yl)
    ylabel('\omega_n [rad/s]')
    grid on
    hold on
    subplot(2,2,2)
    plot(Ro,wnr1(i,:),ls(i,:))
    xlim([min(Ro) max(Ro)])
    xlabel('Footing Radius [m]')
    ylim(yl)
    ylabel('\omega_n [rad/s]')
    grid on
    hold on
    subplot(2,2,3)
    plot(hs,wnh1(i,:),ls(i,:))
    xlim([min(hs) max(hs)])
    xlabel('Sand Depth [m]')
    ylim(yl)
    ylabel('\omega_n [rad/s]')
    grid on
    hold on
    subplot(2,2,4)
    plot(n,wnn1(i,:),ls(i,:))
    xlim([4 16])
    xlabel('Number of Feet')
    ylim(yl)
    ylabel('\omega_n [rad/s]')
    grid on
    hold on
end
hold off
legend('Pak&Guz.','Hardin 63 ','Hardin 63','Seed 86','Iwasaki 78','Oztoprak
13','orientation','horizontal','location','southoutside')
fgn=fgn+1;
%% Plot Relative Damping
yld=[0 1.5];
figure(fgn)
subplot(3,1,1)
plot(Mp,etar1,'r')
xlim([1000 10000])
xlabel('Table Mass [kg]')
ylim(yld)
```

APPENDIX B (CONTINUED)

```
ylabel('relative \eta')
grid on
subplot(3,1,2)
plot(Ro,etar2,'b')
xlim([min(Ro) max(Ro)])
xlabel('Footing Radius [m]')
ylim(yld)
ylabel('relative \eta')
grid on
subplot(3,1,3)
plot(n,etar3,'m')
xlim([4 16])
xlabel('Number of Feet')
ylim(yld)
ylabel('relative \eta')
grid on
fgn=fgn+1;
%% SB Table Results
% Two Comsol Simulations using Parametric studies
Ttf1=IMPSBT('COMDATA/TTF4.txt',9,inf);
Ttf2=IMPSBT('COMDATA/TTF5.txt',9,inf);
fc=Ttf1(:,1);
TFo=Ttf1(:,[2 4])*1e6;
TFo(:,:,2)=Ttf2(:,[2 4])*1e6;
flab=[3.15 4 5 6.3 8 10 12.5 16 20 25 31.5 40 50 63 80 100]; % Preferred
freq. Labels
nfl=length(flab);
x=1:nfl;
NIST=[25e-9*ones(1,9) 3e-6./(flab(10:nfl)*2*pi)];
PSOf=([12.82 11.48 6.26 4.27 4.10 3.18 2.55 2.08 1.77 1.06 1.84 0.349 .160
.666 .0964 .0641;
    6.48 6.19 5.60 6.59 6.53 6.34 5.95 6.99 12.77 7.95 10.53 1.92 0.64 2.05
.298 .136]*1e-9)'; % From Anton 2016
for j=1:2
    PSOt=TFo(:,:,j).*PSOf;
    tt=char('Horizontal (X-direction)','Vertical (Z-direction');
    figure(fgn)
    for i=1:2
        subplot(2,1,i)
        semilogy(x,PSOt(:,i),'go-',x,PSOf(:,i),'bo-');
        hold on
        semilogy(x,NIST,'k')
        hold off
        grid on
        title(tt(i,:))
        ylabel('Displacement [m_r_m_s]')
        if i==2
            xlabel('Freq. [Hz]')
        else
            legend('Table','Floor.','NIST-
A','location','southoutside','orientation','Horizontal')
        end
        ax=gca;
        set(ax,'XTick',x)
```

APPENDIX B (CONTINUED)

```
        set(ax,'XTickLabel',flab)
        xlim([1 nfl])
        ylim([1e-11 1e-7])
    end
    fgn=fgn+1;
end
```

B.2: Code to import FEM data

```
function SBTF = IMPSBT(filename, startRow, endRow)
%IMPORTFILE Import numeric data from a text file as a matrix.
%   TTF5 = IMPORTFILE(FILENAME) Reads data from text file FILENAME for the
%   default selection.
%
%   TTF5 = IMPORTFILE(FILENAME, STARTROW, ENDROW) Reads data from rows
%   STARTROW through ENDROW of text file FILENAME.
%
% Example:
%   TTF5 = importfile('TTF5.txt', 1, 24);
%
%    See also TEXTSCAN.

% Auto-generated by MATLAB on 2018/08/22 11:19:25

%% Initialize variables.
if nargin<=2
    startRow = 1;
    endRow = inf;
end

%% Read columns of data as strings:
% For more information, see the TEXTSCAN documentation.
formatSpec = '%17s%33s%24s%s%[^\n\r]';

%% Open the text file.
fileID = fopen(filename,'r');

%% Read columns of data according to format string.
% This call is based on the structure of the file used to generate this
% code. If an error occurs for a different file, try regenerating the code
% from the Import Tool.
dataArray = textscan(fileID, formatSpec, endRow(1)-startRow(1)+1,
'Delimiter', '', 'WhiteSpace', '', 'HeaderLines', startRow(1)-1,
'ReturnOnError', false);
for block=2:length(startRow)
    frewind(fileID);
    dataArrayBlock = textscan(fileID, formatSpec, endRow(block)-
startRow(block)+1, 'Delimiter', '', 'WhiteSpace', '', 'HeaderLines',
startRow(block)-1, 'ReturnOnError', false);
    for col=1:length(dataArray)
        dataArray{col} = [dataArray{col};dataArrayBlock{col}];
    end
end
```

APPENDIX B (CONTINUED)

```
%% Close the text file.
fclose(fileID);

%% Convert the contents of columns containing numeric strings to numbers.
% Replace non-numeric strings with NaN.
raw = repmat({''},length(dataArray{1}),length(dataArray)-1);
for col=1:length(dataArray)-1
    raw(1:length(dataArray{col}),col) = dataArray{col};
end
numericData = NaN(size(dataArray{1},1),size(dataArray,2));

for col=[1,2,3,4]
    % Converts strings in the input cell array to numbers. Replaced non-
numeric
    % strings with NaN.
    rawData = dataArray{col};
    for row=1:size(rawData, 1);
        % Create a regular expression to detect and remove non-numeric
prefixes and
        % suffixes.
        regexstr = '(?<prefix>.*?)(?<numbers>([-
]*(\d+[\,]*)+[\.]{0,1}\d*[eEdD]{0,1}[-+]*\d*[i]{0,1})|([-
]*(\d+[\,]*)*[\.]{1,1}\d+[eEdD]{0,1}[-+]*\d*[i]{0,1}))(?<suffix>.*)';
        try
            result = regexp(rawData{row}, regexstr, 'names');
            numbers = result.numbers;

            % Detected commas in non-thousand locations.
            invalidThousandsSeparator = false;
            if any(numbers==',');
                thousandsRegExp = '^\d+?(\,\d{3})*\.{0,1}\d*$';
                if isempty(regexp(thousandsRegExp, ',', 'once'));
                    numbers = NaN;
                    invalidThousandsSeparator = true;
                end
            end
            % Convert numeric strings to numbers.
            if ~invalidThousandsSeparator;
                numbers = textscan(strrep(numbers, ',', ''), '%f');
                numericData(row, col) = numbers{1};
                raw{row, col} = numbers{1};
            end
        catch me
        end
    end
end


%% Replace non-numeric cells with NaN
R = cellfun(@(x) ~isnumeric(x) && ~islogical(x),raw); % Find non-numeric
cells
raw(R) = {NaN}; % Replace non-numeric cells
```

APPENDIX B (CONTINUED)

```
%% Create output variable
SBTF = cell2mat(raw);
```

APPENDIX C: MATLAB Code for Embedded Pits

C.1: Main Code

```
% Embedded pits at CNM Building 441
%% Building 441 Ambient Data
% Pit and floor data
close all;  clear;
% Import Data
F=['FLPSA032712075';
'FLPSA031716075';
'P1PSA031312075';
'P1PSA031716075';
'P2PSA032712075';
'P2PSA031716075';
'P2PSA031816075'];
mf=size(F,1);
% Allocate Matrices
C=zeros(3,1);
PS75=zeros(801,7,3);
PO75=zeros(15,5,3);
G=zeros(3201,6,3,2);
nl1=0;
nl2=0;
nlf=0;
config=[3 1 2 2;
    3 1 3 2;
    1 1 1 2;
    1 1 3 2;
    2 1 2 2;
    2 1 3 2;
    2 1 4 2];
loc=char('Pit 1','Pit 2','Floor');
locs=[3 3 1 1 2 2 2];
S=[6.568 7 7.088 7.5 7.39 9.54 7.01;
    ones(1,6) 0;
    7.39 9.71 7.088 9.71 7.01 7.5 0;
    ones(1,6) 0;
    7 7.5 9.54 7.01 7.39 0 0;
    ones(1,6) 0;
    ones(1,6) 0];
r=[3 4 5 11 13 10 12;
    2 3 4 5 6 7 0;
    4 6 7 8 9 10 0;
    2 3 4 5 6 7 0;
    4 6 8 9 10 0 0;
    2 3 4 5 6 7 0;
    2 3 4 5 6 7 0];
Amp=[100*ones(1,7);
    ones(1,5) 10 0;
    100*ones(1,6) 0;
    ones(1,5) 10 0;
    100*ones(1,5) 0 0;
    ones(1,5) 10 0;
    ones(1,5) 10 0];
```

APPENDIX C (CONTINUED)

```
rms=[1.4142 1 1.4142 1.4142 1.4142 1 1]';
for i=1:mf
    % Import Data
    Fo=strcat('EXPDATA/',F(i,:),'.txt');
     D=importdata(Fo);
     % Ambient Power Spec Data
    amb=1;
    rt=nonzeros(r(i,:));
    f=D.data(:,1);
    PS=D.data(:,rt);
    [mt,nt]=size(PS);
    % convert data
    PSD=zeros(mt,nt);
    for j=1:nt;
        PSD(:,j)=1e9*9.81*PS(:,j)./(rms(i)*Amp(i,j)*S(i,j)*(2*pi*f).^2); %
Disp. Power Spetra [nm rms]
    end
    if locs(i)==1
        PS75(:,nl1+1:nl1+nt,locs(i))=PSD;
        nl1=nl1+nt;
    elseif locs(i)==2
        PS75(:,nl2+1:nl2+nt,locs(i))=PSD;
        nl2=nl2+nt;
    else
        PS75(:,nlf+1:nlf+nt,locs(i))=PSD;
        nlf=nlf+nt;
    end
end

flab=[3.15 4 5 6.3 8 10 12.5 16 20 25 31.5 40 50 63 80];
% Plot All Data
PStot75=zeros(801,24,3);
PSOtm=zeros(15,3);
% Ambient Data linear bandwidth and 1/3 octave bands
ML=[50 25 12.5 6.25 3.1 1.56 .78]'; % Max Level for Vibration criteria
[micrron/s, rms]
% VC1=ML(1:2)*[2 2^(2/3) 2^(1/3) ones(1,11)]; % Vibration Criteria A and B
VC2=ML(3:7)*(1./(2*pi*flab))*1e3; % Vibration Criteria C thru G
VClabel='CDEFG';
NISTA=[.025*ones(1,9) 3.1./(2*pi*flab(10:15))]*1e3; % NIST-A Vibration
Criterion
lins=char('-bo','-.b','-.b',':b',':b');
Nfc=length(flab);
x=1:Nfc;
c=-25:-11;
fo=1e3*(2^(1/3).^c); % Center freq.
for k=1:3 % Location
    % All measurements combined for each location
    rt=length(nonzeros(PS75(2,:,k)));
    for j=1:rt
        for i=1:Nfc
            f1=fo(i)/(2^(1/6));
            f2=fo(i)*(2^(1/6));
            if i==Nfc
```

APPENDIX C (CONTINUED)

```
                f2=max(f);
            end
            PSt=zeros(801,1);
            b=1;
            for p=1:801
                if f1<=f(p) && f2>=f(p)
                PSt(b)=PS75(p,j,k);
                b=b+1;
                end
            end
            PSt=nonzeros(PSt);
        %     PSO(k)=rssq(PSt);
            PSOt(i,j)=sqrt(sum(PSt.^2));
        end
    end
    LAm=mean(log(PSOt),2);
    LAstd=std(log(PSOt),0,2);
    Amin=min(PSOt,[],2);
    Amax=max(PSOt,[],2);
    Amps=exp(LAm+LAstd);
    Amms=exp(LAm-LAstd);
    Am=exp(LAm);
    PSOmt=[Am,Amps,Amms,Amax,Amin];
    PSOtm(:,k)=PSOmt(:,2);
    % Ambient Velocity 1/3 oct Spectra
    scrsz = get(groot,'ScreenSize');
    figure('Position',[.5 scrsz(4)/3 scrsz(3)/2 scrsz(4)/2])
    for q=1:5
        semilogy(x,PSOmt(:,q),lins(q,:));
        hold on
    end
    semilogy(1:15,VC2,'--k',1:15,NISTA,'k')
    hold off
    grid on
    legend('Mean','Mean + \sigma', 'Mean -
\sigma','Max','Min','Location','southwest')
    title({'Velocity Power Spectra 1/3 Octave Bands'; loc(k,:);'~'})
    ylabel('Displacement [nm_r_m_s]')
    xlabel('Freq. [Hz]')
    ax=gca;
    set(ax,'XTick',x)
    set(ax,'XTickLabel',flab)
    ylim([2e-1 2e2])
    xlim([1 Nfc])
    for j=1:length(ML(3:7))
        if j==1 || j==2
            xp=8;
        else
            xp=2;
        end
        text(xp,1.25*VC2(j,xp),['VC-',VClabel(j)],'Rotation',-15)
    end
    text(1.25,20,'NIST-A')
end
```

APPENDIX C (CONTINUED)

```
lins2=char('-.o','--o','-o');
scrsz = get(groot,'ScreenSize');
figure('Position',[.5 scrsz(4)/3 scrsz(3)/2 scrsz(4)/2])
for i=1:3
    semilogy(x,PSOtm(:,i),lins2(i,:));
    hold on
end
semilogy(1:15,VC2,'--k',1:15,NISTA,'k')
hold off
grid on
legend('Pit 1','Pit 2','Floor','Location','southwest')
title({'Displacement Power Spectra';'1/3 Octave Bands'; '~'})
ylabel('Displacement [nm_r_m_s]')
xlabel('Freq. [Hz]')
ax=gca;
set(ax,'XTick',x)
set(ax,'XTickLabel',flab)
ylim([2e-1 2e2])
xlim([1 Nfc])
for j=1:length(ML(3:7))
    if j==1 || j==2
        xp=8;
    else
        xp=2;
    end
    text(xp,1.25*VC2(j,xp),['VC-',VClabel(j)],'Rotation',-15)
end
text(1.25,20,'NIST-A')
% Impact Data and FEM
%% Pit 1
ylaba='|g(\omega)| [m/s^2/N]';
ylma=[1e-7 1e-2];
ylri=[-.003 .004];
% Import Exp. Data
F=char('P1COH031312REC','P1TFN031312REC','P1TSR031312REC');
% Force Responce Data
Ft=strcat('EXPDATA/',F(2,:),'.txt');
D=importdata(Ft);
Sac=[7.39 9.71 7.088 9.71 7.01 7.5]; % [V/g] Accelerometer sensitivities
Sh=2.4e-4; % [N/g] Hammer Sensitivity
S=[Sac Sh];
rtf=[4 6 7 8 9 10 14]; % Sensor Channels
Amp=[1 10*ones(1,7)];
% Load Data
TF=D.data;
f=TF(:,1);
n1=length(rtf);
rtf=rtf(1,1:(n1-1));
Gr=TF(:,(2*(rtf-1)));
Gi=TF(:,(2*rtf-1));
for j=1:n1-1
    FRF(:,(2*j-1):2*j)=[Gr(:,j) 1i*Gi(:,j)];
end
[m,nt]=size(Gr);
```

APPENDIX C (CONTINUED)

```
% convert data
% Allocate Matrices
GA=zeros(m,nt);
for q=1:nt;
    if q==2
        GA(:,q)=9.81*FRF(:,q)*S(nt+1)*Amp(nt+1)./(S(q));
    else
        GA(:,q)=9.81*FRF(:,q)*S(nt+1)*Amp(nt+1)./(Amp(q)*S(q));
    end
end
% Moduli of sand
nus=.33;
Dp=1.2192;
L=(15*12+8-4)*.0254; % cap length [m]
B=(12*12+8-4)*.0254; % Cap width [m]
hc1=6*.0254; % cap height [m] (6:5:21)
hs=(4*12+6-hc1)*.0254; % gravel depth [m]
rhos=1560;
Ac=L*B;
Ro=sqrt(Ac/pi);
Vc1=hc1*Ac;
rhoc=3200; % density of concrete [kg/m^3]
mc=rhoc*Vc1;
e=.7;
Est=Esf(Ro,mc,e,nus,1,2:7); % SEE APPENDIX A.2
Estm=mean(Est)
Estd=std(Est)
% Compare Comsol swept parameters vs Exp Data
% Comsol Parameters
Esc2=(1:2:11)*1e6;
etasc2=[.0005 .001];
Esc3=(5:2:15)*1e6;
etasc3=(5:2:9)*1e-5;
Esc4=(11:4:19)*1e6;
etasc4=(1:4:5)*1e-4;
Esc5=(45:5:80)*1e6;
etasc5=1e-4;
Escf=60e6;
etascf=.1;
Esct=Escf;
etasct=etascf;
lE=length(Esct);
leta=length(etasct);
% Import Comsol Data
Gc=COMSWP('COMDATA/P1COMFINAL.txt',9,inf);
lg=length(Gc);
sn1=6;
ld=lg/sn1;
Gca=zeros(ld,sn1);
fc1=Gc(1:ld,1);
cnt=1;
for k=1:sn1
    Gca(:,k)=Gc((ld*(cnt-1)+1):ld*cnt,2);
    cnt=cnt+1;
```

APPENDIX C (CONTINUED)

```
end
% Calculate Error
Il=find(f>=min(fc1),1);
Ih=find(f>=200,1);
Ihc=find(fc1>=200,1);
GAt=GA(Il:3:Ih,:);
SQE=zeros(lE,leta);
for pn1=1:lE
    pd1=strcat('E_s=',num2str(Esct(pn1),'%e'),'Pa');
    for pn2=1:leta
        ER=abs(Gca(:,:,pn1,pn2))-abs(GAt);
        SQEt=ER'*ER; % Squared error error vector (ER) x complex congigate of
ER
        SQE(pn1,pn2)=sum(diag(SQEt));
    end
end
% Plot FEM and Exp Data
[p1m,p2m]=find(SQE==min(min(SQE)));
xl=[3 200];
ylm=[1e-6 1e-2];
ylab='|g(\omega)| [m/s^2/N]';
tt=char(strcat('E_s=',num2str(Esct(p1m)/1e6),'MPa'),strcat('\eta_s=',num2str(
etasct(p2m))));
figure('Position',[.5 scrsz(4)/3 scrsz(3)/3 scrsz(4)/2])
for sn=1:6
    lt=strcat('point-',num2str(sn));
    subplot(3,2,sn)
    semilogy(f,abs(GA(:,sn)),fc1,abs(Gca(:,sn,p1m,p2m)),'g--')
    grid on
    axis([xl ylm])
    if sn==1
        ylabel(ylab)
        title({tt(1,:);lt})
    elseif sn==2
        title({tt(2,:);lt})
    elseif sn==6

legend('Exp.','FEM','location','southoutside','orientation','horizontal')
        title(lt)
    else
        title(lt)
    end
    if sn==3 || sn==5
        ylabel(ylab)
    end
    if sn==5 || sn==6
        xlabel('Frequency [Hz]')
    end
end
%% Pit 2
F=char('P2COH032712REC','P2TFN032712REC','P2TSR032712REC');
mf=size(F,1);
% Force Responce Data
Ft=strcat('EXPDATA/',F(2,:),'.txt');
```

APPENDIX C (CONTINUED)

```
D=importdata(Ft);
Sac2=[7.0 7.5 9.54 7.01 7.39];
S2=[Sac2 Sh];
rtft2=[4 6 8 9 10 14];
Amp2=[1 100*ones(1,5) 10];
% Load Data
TF=D.data;
f=TF(:,1);
n1=length(rtft2);
rtf2=rtft2(1,1:(n1-1));
Gr=TF(:,(2*(rtf2-1)));
Gi=TF(:,(2*rtf2-1));
for j=1:n1-1
    FRF(:,(2*j-1):2*j)=[Gr(:,j) 1i*Gi(:,j)];
end
[m,nt]=size(Gr);
% convert data
GA=zeros(m,nt);
for q=1:nt;
    GA(:,q)=9.81*FRF(:,q)*S2(nt+1)*Amp2(nt+1)./(Amp2(q)*S2(q));
end
GA(:,2)=100*GA(:,2);
% Moduli of sand
nug=.33;
hc2=15*.0254; % cap height [m] (6:5:21)
hg2=(4*12+6-hc2)*.0254; % gravel depth [m]
rhog=1500;
Vc2=hc2*Ac; % [m^2]
mc2=rhoc*Vc2;
Est=Esf(Ro,mc2,e,nug,1,2:7);
Estm2=mean(Est)
Estd2=std(Est)
% Compare Comsol swept parameters vs Exp Data
% Comsol Parameters
Egc1=(50:10:70)*1e6;
etagc1=(3:2:7)*1e-4;
Egc2=70e6;
etagc2=(6.5:.5:9)*1e-4;
Egc3=70*1e6;
etagc3=(5:9)*1e-5;
Egc4=80e6;
etagc4=.04; %eta=loss Mod/storage Mod
Egcf=80e6;
etagcf=.08;
Egct=Egcf;
etagct=etagcf;
lE=length(Egct);
leta=length(etagct);
% Import Comsol Data
Gc=COMSWP('COMDATA/P2COMFINAL.txt',9,inf);
lg=length(Gc);
sn2=5;% number of sensors
ld=lg/sn2;
Gca=zeros(ld,sn2);
```

APPENDIX C (CONTINUED)

```
fc2=Gc(1:ld,1);
cnt=1;
for k=1:sn2
    Gca(:,k)=Gc((ld*(cnt-1)+1):ld*cnt,2);
    cnt=cnt+1;
end
% Calculate Error
Il=find(f>=min(fc2),1);
Ih=find(f>200,1);
Ihc=find(fc2>=200,1);
GAt=GA(Il:3:Ih,:);
Gcat=Gca(1:Ihc,:,:,:);
SQE=zeros(lE,leta);
for pn1=1:lE
    pd1=strcat('E_s=',num2str(Egct(pn1),'%e'),'Pa');
    for pn2=1:leta
        ER=abs(Gcat(:,:,pn1,pn2))-abs(GAt);
        SQEt=ER'*ER; % Squared error error vector (ER) x complex congigate of
ER
        SQE(pn1,pn2)=sum(diag(SQEt));
    end
end
[p1m,p2m]=find(SQE==min(min(SQE)));
Ef=Egct(p1m);
etagf=etagct(p2m);
tt=char(strcat('E_g=',num2str(Egct(p1m)/1e6),'MPa'),strcat('\eta_g=',num2str(
etagct(p2m))));
xl=[3 200];
ylm=[1e-6 1e-2];
ylab='|g(\omega)| [m/s^2/N]';
figure('Position',[.5 scrsz(4)/3 scrsz(3)/3 scrsz(4)/2])
for sn=1:5
    lt=strcat('point-',num2str(sn));
    subplot(3,2,sn)
    semilogy(f,abs(GA(:,sn)),fc2,abs(Gca(:,sn,p1m,p2m)),'g--')
    grid on
    axis([xl ylm])
    if sn==1
        ylabel(ylab)
        title({tt(1,:);lt})
        legend('Exp.','FEM')
    elseif sn==2
        title({tt(2,:);lt})
    else
        title(lt)
    end
    if sn==3 || sn==5
        ylabel(ylab)
    end
    if sn==5 || sn==6
        xlabel('Frequency [Hz]')
    end
end
```

APPENDIX C (CONTINUED)

C.2: Code to calculate Young's modulus from theoretical equations

*See **Appendix A.2***

C.3: Code to import FEM data

```
function GAc = COMSWP(filename, startRow, endRow)
%IMPORTFILE Import numeric data from a text file as a matrix.
%   P1COMSWP1 = IMPORTFILE(FILENAME) Reads data from text file FILENAME for
%   the default selection.
%
%   P1COMSWP1 = IMPORTFILE(FILENAME, STARTROW, ENDROW) Reads data from rows
%   STARTROW through ENDROW of text file FILENAME.
%
% Example:
%   P1COMSWP1 = importfile('P1COMSWP1.txt', 1, 28250);
%
%    See also TEXTSCAN.

% Auto-generated by MATLAB on 2018/05/27 12:21:42

%% Initialize variables.
if nargin<=2
    startRow = 1;
    endRow = inf;
end

%% Read columns of data as strings:
% For more information, see the TEXTSCAN documentation.
formatSpec = '%19s%s%[^\n\r]';

%% Open the text file.
fileID = fopen(filename,'r');

%% Read columns of data according to format string.
% This call is based on the structure of the file used to generate this
% code. If an error occurs for a different file, try regenerating the code
% from the Import Tool.
dataArray = textscan(fileID, formatSpec, endRow(1)-startRow(1)+1,
'Delimiter', '', 'WhiteSpace', '', 'HeaderLines', startRow(1)-1,
'ReturnOnError', false);
for block=2:length(startRow)
    frewind(fileID);
    dataArrayBlock = textscan(fileID, formatSpec, endRow(block)-
startRow(block)+1, 'Delimiter', '', 'WhiteSpace', '', 'HeaderLines',
startRow(block)-1, 'ReturnOnError', false);
    for col=1:length(dataArray)
        dataArray{col} = [dataArray{col};dataArrayBlock{col}];
    end
end

%% Close the text file.
fclose(fileID);
```

APPENDIX C (CONTINUED)

```
%% Convert the contents of columns containing numeric strings to numbers.
% Replace non-numeric strings with NaN.
raw = repmat({''},length(dataArray{1}),length(dataArray)-1);
for col=1:length(dataArray)-1
    raw(1:length(dataArray{col}),col) = dataArray{col};
end
numericData = NaN(size(dataArray{1},1),size(dataArray,2));

for col=[1,2]
    % Converts strings in the input cell array to numbers. Replaced non-
numeric
    % strings with NaN.
    rawData = dataArray{col};
    for row=1:size(rawData, 1);
        % Create a regular expression to detect and remove non-numeric
prefixes and
        % suffixes.
        regexstr = '(?<prefix>.*?)(?<numbers>([-
]*(\d+[\,]*)+[\.]{0,1}\d*[eEdD]{0,1}[-+]*\d*[i]{0,1})|([-
]*(\d+[\,]*)*[\.]{1,1}\d+[eEdD]{0,1}[-+]*\d*[i]{0,1}))(?<suffix>.*)';
        try
            result = regexp(rawData{row}, regexstr, 'names');
            numbers = result.numbers;

            % Detected commas in non-thousand locations.
            invalidThousandsSeparator = false;
            if any(numbers==',');
                thousandsRegExp = '^\d+?(\,\d{3})*\.{0,1}\d*$';
                if isempty(regexp(thousandsRegExp, ',', 'once'));
                    numbers = NaN;
                    invalidThousandsSeparator = true;
                end
            end
            % Convert numeric strings to numbers.
            if ~invalidThousandsSeparator;
                numbers = textscan(strrep(numbers, ',', ''), '%f');
                numericData(row, col) = numbers{1};
                raw{row, col} = numbers{1};
            end
        catch me
        end
    end
end


%% Replace non-numeric cells with NaN
R = cellfun(@(x) ~isnumeric(x) && ~islogical(x),raw); % Find non-numeric
cells
raw(R) = {NaN}; % Replace non-numeric cells

%% Create output variable
      GAc = cell2mat(raw);
```

VITA

Jayson WJ Anton

Education

Bachelor of Science, Mechanical Engineering, Oregon State University, 2005
Doctor of Philosophy, Mechanical Engineering, University of Illinois at Chicago, 2018

Experience

Advanced Photon Source, Argonne National Laboratory, Argonne, Illinois 2009-present
X-ray Science Division, Nano-positioning group, Guest Graduate

University of Illinois at Chicago, 842 W. Taylor St., Chicago, IL 60607 2009-present
Dept. of Mechanical and Industrial Engineering, Graduate Research Assistant

Publications and Presentations

Anton, **Jayson**, Steven Kearney, and Deming Shu, "Ambient Vibration Measurement in Sectors 29," in 2017 APS/CNM Users Meeting, May 2017.

Anton, **Jayson**, Steven Kearney, Vincent De Andrade, Alex Deriy, and Deming Shu. "Ambient Vibration Measurement for APS 32-ID-C Floor, Table, and Sample Stages." (2016).

Anton, **Jayson**, Steven Kearney, and Deming Shu. "Ambient Vibration Measurement for APS floor at Sectors 29, 26, 23, and 21." (2016).

Shu, Deming, Barry Lai, Steven Kearney, **Jayson Anton**, Wenjun Liu, Jorg Maser, Christian Roehrig, and Jonathan Z. Tischler. "Design and test of precision vertical and horizontal linear nanopositioning flexure stages with centimeter-level travel range for x-ray instrumentation." In *Optomechanical Engineering 2017*, vol. 10371, p. 103710C. International Society for Optics and Photonics, 2017.

Shu, Deming, B. Lai, Steven Kearney, **J. Anton**, Wenjun Liu, J. Maser, Chris Roehrig, and J. Z. Tischler. "Mechanical design of compact vertical and horizontal linear nanopositioning flexure stages with centimeter-level travel range for x-ray beamline instrumentation." *Proceedings of IPAC2017, Copenhagen, Denmark, THPAB154, ISBN* (2017): 978-3.

Shu, Deming, Yaolin Pan, Chengwen Mao, Aiguo Li, **Jayson Anton**, and Steven Kearney. "Precision Mechanical Design of a Miniature Dynamic Mirror Bender for the SSRF Beamline Upgrade Project." (2017): TUAA01.

Shu, Deming, Steven Kearney, Barry Lai, Chris Roehrig, Jonathan Tischler, Wenjun Liu, **Jayson Anton**, and J. Ã. Maser. "Mechanical design and development of compact linear nanopositioning flexure stages with centimeter-level travel range and nanometer-level resolution." (2017): TUBA04.

Shu, Deming, Yaolin Pan, Chengwen Mao, Aiguo Li, **Jayson Anton**, and Steven Kearney. "Precision Mechanical Design of a Miniature Dynamic Mirror Bender for the SSRF Beamline Upgrade Project." (2017): TUAA01.

Shu, D., J. Qian, W. Liu, S. Kearney, **J. Anton**, J. Sullivan, and L. Assoufid. "Design of a precision two-dimensional tip-tilting stage system for autocollimator-based long trace profiler angular calibration." In *Advances in Metrology for X-Ray and EUV Optics V*, vol. 9206, p. 92060H. International Society for Optics and Photonics, 2014.

Shu, D., S. Kalbfleisch, S. Kearney, **J. Anton**, and Y. S. Chu. "Optomechanical design of a high-precision detector robot arm system for x-ray nano-diffraction with x-ray nanoprobe." In *Journal of Physics: Conference Series*, vol. 493, no. 1, p. 012027. IOP Publishing, 2014.

Shu, D., S. Kalbfleisch, S. Kearney, **J. Anton**, and Y. S. Chu. "Optomechanical design of a high-precision detector robot arm system for x-ray nano-diffraction with x-ray nanoprobe." In *Journal of Physics: Conference Series*, vol. 493, no. 1, p. 012027. IOP Publishing, 2014.

Shu, D., R. Harder, J. Almer, N. Kujala, S. Kearney, **J. Anton**, W. Liu et al. "Optomechanical design of a modular KB mirror mount system for x-ray microfocusing at the advanced photon source." In *Optomechanical Engineering 2013*, vol. 8836, p. 88360O. International Society for Optics and Photonics, 2013.